

Ing. Khanh Duong Quang

Summary of doctoral dissertation

MOTION CONTROL OF MULTI-AXIAL VIBRATIONAL MECHATRONIC SYSTEMS

Submitted for the degree of doctor (Philosophiae Doctor, PhD.)

in the doctoral study programme: Robotics and Cybernetics

in the study field: 9.2.7 Cybernetics

Place and date: Bratislava, January 10th, 2016

**SLOVAK UNIVERSITY OF TECHNOLOGY IN BRATISLAVA
FACULTY OF ELECTRICAL ENGINEERING AND INFORMATION TECHNOLOGY**

Ing. Khanh Duong Quang

Summary of doctoral dissertation

MOTION CONTROL OF MUTLI-AXIAL VIBRATIONAL MECHATRONIC SYSTEMS

Submitted for the degree of doctor (Philosophiae Doctor, PhD.)

in the doctoral study programme:

Robotics and cybernetics

Place and date: Bratislava, January 10th, 2016

The dissertation thesis was developed in the full-time doctoral study form

At: Institute of Robotics and Cybernetics
Faculty of Electrical Engineering and Information Technology
Slovak University of Technology in Bratislava
Ilkovičová 3, 81219 Bratislava, Slovak Republic

Author: **Ing. Khanh Duong Quang**
Institute of Robotics and Cybernetics
Faculty of Electrical Engineering and Information Technology
Slovak University of Technology in Bratislava
Ilkovičová 3, 81219 Bratislava, Slovak Republic

Supervisor: **Prof. Ing. Peter Hubinský, PhD.**
Institute of Robotics and Cybernetics
Faculty of Electrical Engineering and Information Technology
Slovak University of Technology in Bratislava
Ilkovičová 3, 81219 Bratislava, Slovak Republic

Opponents: **Prof. Ing. Aleš Janota, PhD.**
Faculty of Electrical Engineering
University of Zilina
Prof. Ing. Cyril Belavý, PhD.
Faculty of Mechanical Engineering
Slovak University of Technology in Bratislava

Summary of dissertation was submitted on:

Dissertation defense will be taken place on:

At Institute of Robotics and Cybernetics, Faculty of Electrical Engineering and
Information Technology
Slovak University of Technology in Bratislava
Ilkovičová 3, 81219 Bratislava, Slovak Republic

Prof. Dr. Ing. Miloš Oravec
Dean of Faculty
Slovak University of Technology in Bratislava

TABLE OF CONTENTS

Chapter 1 Introduction	1
1.1 Overview	1
1.2 The objectives of dissertation	3
Chapter 2 Input shaping	4
2.1 Off-line shaping	4
2.2 On-line shaping	4
2.3 Input shaper with positive amplitudes	5
2.4 Input shaper with negative amplitudes	6
2.5 Genetic algorithm based input shaping	6
2.6 Implementation of input shaper in the discrete domain	7
Chapter 3 NURBS curve representation	9
3.1 Definition and properties of NURBS curves	9
3.2 Derivatives of a NURBS curve	10
Chapter 4 NURBS interpolation and feedrate planning	11
4.1 Introduction	11
4.2 Natural interpolation	12
4.3 Taylor expansion interpolation	12
4.4 Feed correction polynomial	13
4.5 Adaptive feedrate	13
4.6 Feedrate scheduling	14
Chapter 5 Identification of system parameters	16
5.1 Introduction	16
5.2 Grid encoder	16
5.3 Accelerometer	18
Chapter 6 Simulations	21
6.1 Introduction	21
6.2 Tracking and contouring error	21
6.3 Drive controller	23
6.4 Square	23
6.5 Circle	24
6.6 The ∞ shape toolpath	26
6.7 Arbitrary shape toolpath	28
Chapter 7 Experimental results	32

7.1	Hardware	32
7.2	Square	33
7.3	Circle	33
7.4	The ∞ shape toolpath	36
7.5	Arbitrary toolpath	38
CONCLUSIONS		40
REFERENCE		41

Chapter 1 Introduction

1.1 Overview

In industrial machining, demands on high speed and high accuracy require researchers to study the fields such as: parametric curve interpolation, feed profile scheduling, servo-loop control techniques. In recent years, Non Uniform Rational B-Splines (NURBS) have been adopted to CAD/CAM systems and are considered as a fundamental geometry representation. NURBS offer a common mathematical form for representing and designing both standard analytical shapes and free-form curves, surfaces [1]. NURBS reveal the advantages in comparison with conventional parametric curve representation because of their smoothness, flexibility of the toolpath. Most conventional CNC machines provide linear or circular interpolation, the cutting path is given by a set of lines. Therefore, for high precision machining a number of cutting points are required to be increased. Consequently, data transmission speed between CAD/CAM systems and CNC machine is higher and with the limited capacity of memory storage transferred data can be lost. Since using NURBS curve representation, an amount of data exchange is decreased significantly because only the values of control points, knot vector and weight coefficients are transferred from CAD/CAM system to CNC machines. The main problem with the use of NURBS interpolation technique is that the length of NURBS segments is unknown analytically. The discrepancy between the spline parameter and the actual arc length results in undesired feed fluctuations during real time interpolation. Feed fluctuations can bring high accelerations and jerks to the motor and lead to possibilities of drive excitations, finally deteriorate the overall curve or surface quality. To eliminate feed fluctuation, many papers have been proposed to solve this problem. Shpitalni and Koren [2, 3] proposed Taylor's expansion method to develop the first-order and the second-order interpolation algorithm while maintaining the constant feedrate. Taylor's expansion interpolation contributes to the significant improvement over natural interpolation for a generic parametric curve. Nevertheless, the existence of the derivative computation and a square root operation increases the computational load in the real-time system. Moreover, the method is exact only when the parametric curve is sufficiently smooth and the first derivative of the curve is continuous. The curve fitting would encounter numerical issues when the curve has small radii of curvature. Erkorkmaz et al. [4, 5] proposed feed correction polynomial (a 7th order polynomial) to parameterize the relationship between the arc length and the spline parameter. Single feed correction polynomial would encounter the same problem as Taylor's expansion method. To avoid this problem they used multiple feed correction polynomials instead of increasing the order of the polynomial.

In the machining process, feed profile generation can be viewed as offline part. Obviously, optimization of feed profiles also plays a major role in achieving the high precision of freeform

toolpath. The feed modulation strategy needs to be able to travel adaptively along the toolpath in consideration of the local curvature while preserving the physical constraints of the machine tools. Weck et al. [6] presented a worst-case optimization technique in which the maximum allowable feedrate for each segment is computed considering the feed limit, acceleration limit and jerk limit of the machine tools. The method has a straightforward formulation and requires short time of computation so it is convenient in real time CNC interpolators. Since at some sections of the curve the higher feasible feeds are not selected as the utilized ones, the total cycle time is not totally optimized. Some authors have attempted to optimize the maximum allowable feed by using numerical optimization techniques [8, 9].

Even when the designed NURBS curve for the CAD/CAM system is considered accurate which means feedrate fluctuation is completely eliminated, implementation of driving mechanism can still lead the overall system to structural excitation mode. Vibration occurs due to the physical deformation of the structure in the links or joints and again results in reducing the positioning accuracy of the machines. Input shaping is a feed-forward method which effectively depresses vibration. Input shaping is based on the convolution of the desired input and a sequence of Dirac impulses to produce a shaped reference input. Most publications refer the impulse sequence to input shaper. The method performs more effectively for vibration reduction when applying ZVD, EI shapers instead of ZV shaper due to robustness to modeling errors. These shapers are derived by solving a set of constraints which express the residual vibration of the system [14, 15]. The system has more robustness when the number of impulses in the sequence is increased, but the total delay time is added to the overall system process. Similarly, Hubinsky et al. [16, 17] supposed numerical approach using genetic algorithms (GA) to determine the parameters of input shaper. Based on the same idea, Duong et al. [18] investigated the feasibility of GA based input shaper application on an arbitrary NURBS trajectory by means of tracking error.

This work is categorized into seven chapters. Chapter 1 introduces the review of the related literatures and the objectives of the dissertation. Chapter 2 presents the various types of input shaper designed by both analytical and numerical approaches. The NURBS curve representation is described in Chapter 3 as the mathematical tool to generate a smooth toolpath. The real time interpolation methods for NURBS toolpaths and feed planning algorithms are mentioned in Chapter 4. In this thesis, the idea of feed correction polynomial interpolation is employed to capture the relationship between the arc length and the spline parameter for arbitrary trajectory machining. The worst-case method was adopted to generate the feed profile because of the simplicity in computation and wide application in industry. The system parameters of the concrete biaxial CNC machine are identified in Chapter 5 using either the high precision of the machining tool KGM 182 grid encoder or the MEMS linear acceleration

sensor LSM303DLHC. Well-known vibration parameters are then applied to design all the mentioned types of input shapers. The system model is simulated in Chapter 6 under consideration of axis feed drive dynamics. Different shapes of the toolpath such as the square, the circle, the ∞ shape toolpath, the arbitrary NURBS toolpath are chosen to investigate the effectiveness of input shaping on trajectory following. The generated positions in Matlab/Simulink environment are used as input commands for the real time CNC machine MSF1863 using laser. The experimental results with the use of input shaping technique are illustrated and compared to that without in Chapter 7.

The contribution of this work is to verify the effectiveness of input shaping for vibration reduction in the real time high speed CNC machine. The disadvantage of input shaping is to add a delay to the overall system. By making some simple adjustments to the unshaped command, the performance with shaping is superior to that without shaping for contouring errors. When the curve is generated using NURBS interpolation technique, genetic algorithm based input shaper has demonstrated better than other conventional shapers in terms of the presented trajectory following. However, numerical method based shaper has to pay at the expense of highly computational time.

1.2 The objectives of dissertation

The main objectives of this dissertation are:

- 1.To create a mathematical model for the concrete type of multi-axial mechatronic system where vibration occurs at the endpoint of the machine's tool.
- 2.To identify the vibration parameters of the given multi-axial mechatronic system using MEMS inertial sensor.
- 3.To propose a method of trajectory generation in 2D or 3D space enabling to suppress vibration while maintaining the specified trajectory and velocity profile within the specified allowable tolerance.
- 4.To implement the proposed algorithms in the real-time mechatronic system and compare their effectiveness.

Chapter 2 Input shaping

2.1 Off-line shaping

Input shaping can be classified into two categories: off-line and on-line shaping. Off-line shaping is the command profile generation method in order to induce no vibration on the output response. In that, the common command profiles as triangular, trapezoidal, bang coast bang profile are applied to the systems which use repeatedly the same command for their movement cycle such as motor drive used in printer, hard disk, etc. For these systems, the switch times of acceleration and deceleration must be determined in advance and saved in the table that is used later for velocity planning. As all real systems have limits, motion planning requires specifications of the servo limitations on velocity and acceleration. Appropriate command generation can prevent the system to excite. Its frequency content in acceleration and jerk can be demonstrated using Fourier transform.

2.2 On-line shaping

On-line shaping is the in advance unknown command generation profile pre-shaping method. The principle of input shaping is based on the convolution of an impulse sequence (named as input shaper) with the desired system command to produce the shaped input. The result product is then used as input signal to drive the system.

In mathematical representation, input shaper is defined as a sequence of Dirac delta function.

$$IS(t) = \sum_{i=1}^n A_i \delta(t - t_i), \quad 0 \leq t_i \leq t_{i+1}, \quad A_i \neq 0 \quad (2.1)$$

where $\delta(t)$ is the Dirac delta function, A_i is the amplitude of the i -th impulse, t_i is the time shift of the i -th impulse.

The transfer function of an under-damped second-order system with an undamped natural frequency of ω_n and a damping ratio of ζ can be generally described by:

$$F(s) = \frac{\omega_n^2}{s^2 + 2\zeta\omega_n s + \omega_n^2} \quad (2.2)$$

A mathematical formula of residual vibration results from a sequence of impulses which is applied on underdamped second-order system (2.2) is:

$$V(\omega_n, \zeta) = e^{-\zeta\omega_n t_n} \sqrt{[C(\omega_n, \zeta)]^2 + [S(\omega_n, \zeta)]^2} \quad (2.3)$$

To assure the shaper has unity gain, sum of impulse amplitudes must be equal to unity:

$$\sum_{i=1}^n A_i = 1 \quad (2.4)$$

2.3 Input shaper with positive amplitudes

Limiting the impulse amplitudes to be positive facilitates the specification of input shapers. We have to pay for worse performance in rise time when the impulse sequence length is longer than that using negative amplitude. However, energy consumption for motor to move in the transient state is less.

The problem with the use of positive impulse amplitudes can be stated as: find an impulse sequence that satisfies the constraints (2.3), (2.4) and each impulse amplitude must be constrained: $0 \leq A_i \leq 1$. If the number of impulses in the input shaper is two, the solution for impulse parameters is unique. The shaper is called Zero Vibration (ZV). The ZV shaper is often very sensitive to the uncertainties of modeling error and system nonlinearities. Hence, it is not effective on the real systems. For increasing insensitivity to modeling errors, multiple zeros are required to be placed exactly at the system poles. This type of input shaper is called Zero Vibration Derivation (ZVD) shaper. By placing zeros in the neighborhood of the flexible poles Extra-Insensitive (EI) shaper can be derived.

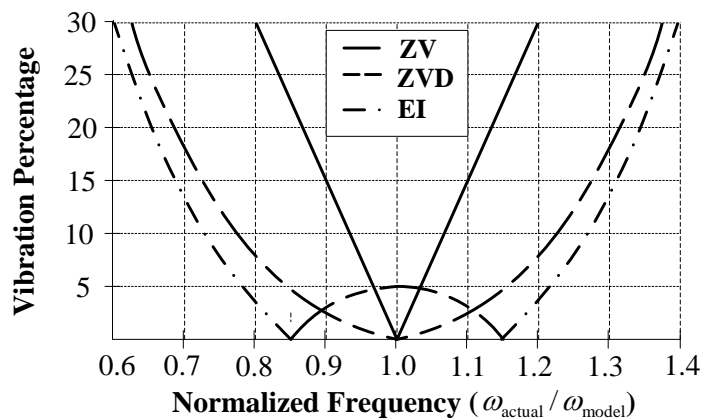


Figure 2.1: Sensitivity curves for ZV, ZVD, EI shapers

The robustness of an input shaper can be quantitatively evaluated by measuring the width of its sensitivity curve. Figure 2.1 plots the sensitivity for various input shapers: ZV, ZVD, EI shapers. Both ZVD and EI shapers have a time duration equal to one period of vibration. However, EI shaper has

a greater width of the insensitivity curve in low level of vibration than ZVD shaper, for example for allowable limit value $V = 5\%$.

2.4 Input shaper with negative amplitudes

As we have discussed above, all three types of input shapers contain positively valued impulses. When the impulses with negative amplitudes are allowed, the shaper length can be greatly reduced. A sequence using negative impulses is referred to a negative sequence. A problem often occurs with negative sequences that they may generate commands that sometimes exceed actuator limits. For a positive sequence, the amplitude of the shaped command never exceeds the maximum amplitude of the unshaped command due to the constraint (2.4).

2.5 Genetic algorithm based input shaping

Genetic algorithm (GA) is an optimization and search technique based on the principles of genetics and natural selection, such as inheritance, mutation, selection and crossover. A GA allows a population composed of many individuals to evolve under specified selection rules to a state that maximizes (minimizes) the cost function [22]. If we consider the system residual vibration to be the cost function, so GA can help us search the optimal amplitudes and time locations of impulse shapers. Assume that each chromosome has N_i amplitudes and N_i time locations of an impulse sequence.

$$chromosome = [A_1, \dots, A_{N_i}, T_1, \dots, T_{N_i}] \quad (2.5)$$

The general conditions required for impulse sequence are their amplitudes and time locations must satisfy the equation (2.4) to preserve the final setpoint. So the task of our work can be formed as: solve for amplitudes and time locations such that satisfying the equation (2.4) and the objective function of residual vibration is optimized (minimized).

$$\begin{aligned} Objective\ Function &= f(chromosome) \\ \text{Subject to the constraint: } &\sum_{i=1}^{N_i} A_i = 1 \end{aligned} \quad (2.6)$$

A new objective function can be formed either by following position or velocity. For some certain cases, their combination with a weight coefficient is also used when the position and velocity are taken account into. However, the selection of appropriate weight coefficients is not easy. Obviously, it depends on the consideration whether position errors or velocity errors are more weighted.

In comparison to the analytical method, finding the parameters of input shaper based on GA approach has some advantages. The shaper parameters are not calculated as functions of damping ratio.

Input shaping

So GA based input shaping avoids solving a set of simultaneous transcendental equations that are complicated to be solved by analytic method. On the contrary, the GA based input shaping also has the weak points. For a specific vibration system the GA approach requires a huge amount of computations. Since solved by the numerical approach, there exists no generic expression designed for GA based input shaper. Secondly, the searching process may get stuck when the amplitudes and time locations of impulse sequence are limited by the large range

2.6 Implementation of input shaper in the discrete domain

All three common types of input shaper mentioned above were designed in the s-plane by the analytical approach. They are then implemented digitally by using a computer to perform the convolutions. If the location times of impulse are not placed at multiple of the discrete sampling time T_s , the computed times would be rounded. This would lead to inexact product convolution. A method should be proposed to overcome the problem.

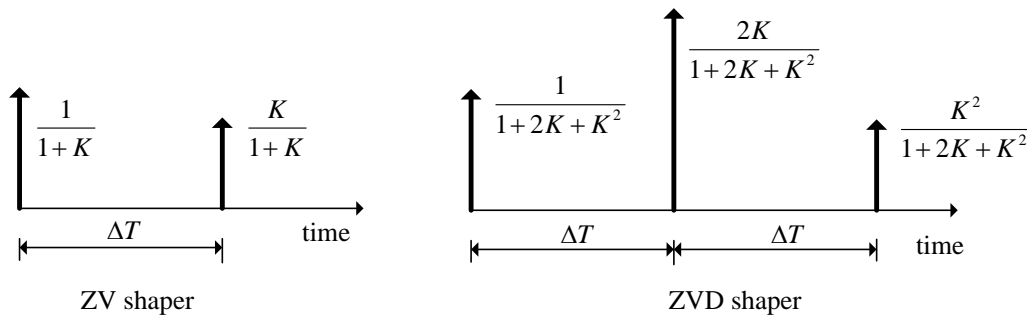


Figure 2.2: ZV and ZVD shaper

In Figure 2.2, K is given as in (2.7), ΔT is one half period of damped vibration:

$$\Delta T = \frac{\pi}{\omega_n \sqrt{1-\zeta^2}}, \quad K = e^{-\frac{\zeta\pi}{\sqrt{1-\zeta^2}}} \quad (2.7)$$

By taking z transform, ZV and ZVD shapers are described in the z plane as follows:

$$IS_{ZV}(z) = \frac{1}{1+K} + \frac{Kz^{-n}}{1+K} \quad (2.8)$$

$$IS_{ZVD}(z) = \frac{1+2Kz^{-n}+K^2z^{-2n}}{1+2K+K^2} \quad (2.9)$$

where $n = \frac{\Delta T}{T_s}$. If the sampling time T_s equals to ΔT ($n=1$), the filter in (2.8) is called a first order digital shaping filter and the filter in (2.9) is a second order digital shaping filter.

The design of EI shaper is transformed to the z-plane as:

$$IS_{EI}(z) = A_1 + A_2 z^{-n_2} + A_3 z^{-n_3} \quad (2.10)$$

where $n_2 = \frac{T_2}{T_s}$, $n_3 = \frac{T_3}{T_s}$; T_2 , T_3 are the time locations of the second and third impulse in an EI shaper;

A_1 , A_2 , A_3 are the first, the second and the third impulse amplitude respectively. Input shapers based on genetic algorithm are also implemented digitally as EI shapers. If the rate between the sample period and one half period of vibration is small enough, impulses can be simply approximated as located at the sample times.

In the discrete domain, Tuttle [21] used zero-placement technique to derive the discrete input shaper. That is, shaper zeros must be placed at the location of the poles. For increasing robustness, additional zeros can be placed at or near the poles. The shaper transfer function containing four zeros as well as poles in the z-plane is given by:

$$IS_{zp}(z) = C \frac{(z - z_1)(z - z_1^*)(z - z_2)(z - z_2^*)}{z^4} = C \frac{z^4 + a_1 z^3 + a_2 z^2 + a_3 z + a_4}{z^2} \quad (2.11)$$

where

$$\begin{aligned} a_1 &= -2(R_1 \cos \theta_1 + R_2 \cos \theta_2) \\ a_2 &= R_1^2 + 4R_1 R_2 \cos \theta_1 \cos \theta_2 + R_2^2 \\ a_3 &= -2(R_1 R_2^2 \cos \theta_1 + R_1^2 R_2 \cos \theta_2) \\ a_4 &= R_1^2 R_2^2 \end{aligned} \quad (2.12)$$

$$\begin{aligned} R_1 &= \exp(-\zeta \omega_{n1} \Delta T) \\ \theta_1 &= \Delta T \omega_{n1} \sqrt{1 - \zeta^2} \\ R_2 &= \exp(-\zeta \omega_{n2} \Delta T) \\ \theta_2 &= \Delta T \omega_{n2} \sqrt{1 - \zeta^2} \end{aligned}$$

C is the constant and used to assure the unity gain of the impulse amplitudes. ω_{n1} , ω_{n2} are the modeling frequencies for each mode if the system has two modes of vibration or estimated modeling frequencies equal or near the real natural frequency if the system has only one mode. In comparison to other methods, the zero-placement (ZP) technique has the advantage in terms of design in the discrete domain because impulses are placed exactly at multiples of the sampling time T_s . The designed two mode shaper is then transformed into the time domain as:

$$IS_{zp}(t) = C(\delta(t) + a_1 \delta(t - \Delta T) + a_2 \delta(t - 2\Delta T) + a_3 \delta(t - 3\Delta T) + a_4 \delta(t - 4\Delta T)) \quad (2.13)$$

Chapter 3 NURBS curve representation

3.1 Definition and properties of NURBS curves

Non Uniform Rational B-Splines (NURBS) have become powerful tools for geometry representation. NURBS offer great flexibility and precision for representing both analytic shapes and free-form curves, surfaces [1]. Due to the advantages, NURBS are not only used in computer graphics, but also in the modern CAD/CAM/CAE systems. NURBS are generalizations of both Bézier and B-splines curves and surfaces. More precisely, Bézier representation is the special case of B-splines representation with a knot vector having two knots. Another important property of NURBS curves and surfaces is that they are invariant under common geometric transformations such as translation, rotation, parallel and perspective projections.

A p -degree NURBS curve is defined by [1]:

$$\mathbf{C}(u) = \begin{bmatrix} x(u) \\ y(u) \\ z(u) \end{bmatrix} = \frac{\sum_{i=0}^n N_{i,p}(u) w_i \mathbf{P}_i}{\sum_{i=0}^n N_{i,p}(u) w_i}, \quad a \leq u \leq b \quad (3.1)$$

where $\{\mathbf{P}_i\}$ are the control points, the $\{w_i\} > 0$ are the weights, $\{N_{i,p}(u)\}$ are the p -th degree B-spline basis functions defined recursively on the non-periodic and non-uniform knot vector

$U = \left\{ \underbrace{a, \dots, a}_{p+1}, u_{p+1}, \dots, u_{m-p-1}, \underbrace{b, \dots, b}_{p+1} \right\}$ as follows:

$$N_{i,0}(u) = \begin{cases} 1 & \text{if } u_i \leq u < u_{i+1} \\ 0 & \text{otherwise} \end{cases} \quad (3.2)$$

$$N_{i,k}(u) = \frac{u - u_i}{u_{i+p} - u_i} N_{i,k-1}(u) + \frac{u_{i+1} - u}{u_{i+p+1} - u_{i+1}} N_{i+1,k-1}(u)$$

We often assume $a = 0, b = 1$ for all cases of computation. A NURBS curve can also be rewritten in the form with no absence of denominator:

$$\mathbf{C}(u) = \sum_{i=0}^n R_{i,p}(u) \mathbf{P}_i \quad (3.3)$$

where the rational basis functions $\{R_{i,p}(u)\}$ are defined as:

$$R_{i,p}(u) = \frac{N_{i,p}(u)w_i}{\sum_{i=0}^n N_{i,p}(u)w_i} \quad (3.4)$$

$\{R_{i,p}(u)\}$ are the rational basis functions which are piecewise rational functions on $u \in [0,1]$. This form helps us compute derivatives of NURBS curves in terms of derivatives of NURBS curves. The degree p , the number of knots $m+1$ and the number of control points $n+1$ are related by the equation: $m = n + p + 1$.

3.2 Derivatives of a NURBS curve

Computation of derivatives of a NURBS curve plays an important role in the curve continuity and smoothness study. Complete feedrate planning should take into account the local curvatures of a NURBS curve, which are also computed in terms of the first and the second derivative of a NURBS curve. Derivatives of rational B-spline curves are more complicated than in case of non-rational B-spline curves because of involving denominator to high powers. In the equivalent form (3.3), a NURBS curve is represented by rational basis functions. Derivatives of a NURBS curve are then given by computing derivatives of each rational basis function $R_{i,p}(u)$:

$$\mathbf{C}^{(k)}(u) = \begin{bmatrix} x^{(k)}(u) \\ y^{(k)}(u) \\ z^{(k)}(u) \end{bmatrix} = \sum_{i=0}^n R_{i,p}^{(k)}(u) \mathbf{P}_i \quad (3.5)$$

For example, the first and the second derivative of rational basis functions are computed by (3.6), (3.7) respectively.

$$R_{i,p}^{(1)}(u) = \frac{N_{i,p}^{(1)}(u)w_i}{\sum_{i=0}^n N_{i,p}(u)w_i} - \frac{N_{i,p}(u)w_i \sum_{i=0}^n N_{i,p}^{(1)}(u)w_i}{\left(\sum_{i=0}^n N_{i,p}(u)w_i \right)^2} \quad (3.6)$$

$$R_{i,p}^{(2)}(u) = \frac{N_{i,p}^{(2)}(u)w_i}{\sum_{i=0}^n N_{i,p}(u)w_i} + \frac{2N_{i,p}(u)w_i \left[\sum_{i=0}^n N_{i,p}^{(2)}(u)w_i \right]}{\left[\sum_{i=0}^n N_{i,p}(u)w_i \right]^3} - \frac{\left[2N_{i,p}^{(1)}(u)w_i \sum_{i=0}^n N_{i,p}^{(1)}(u)w_i + N_{i,p}(u)w_i \sum_{i=0}^n N_{i,p}^{(2)}(u)w_i \right]}{\left[\sum_{i=0}^n N_{i,p}(u)w_i \right]^2} \quad (3.7)$$

Chapter 4 NURBS interpolation and feedrate planning

4.1 Introduction

The spline toolpath is interpolated in real time at every sampling control step of servo controller. The interpolation process provides a sequence of reference points for the position tracking loop of CNC servo system. Conventional CNC machines use common interpolation techniques: linear, arc, cubic or quintic interpolation. The cutter path is then given by a set of lines. Therefore, for accurate machining data transmission load between CAD/CAM systems and CNC machines is increased. Since using NURBS curve representation, a large amount of data exchange is decreased because only the values of control points, knot vector and weight coefficients are needed to be transferred. The main problem with the use of NURBS interpolation techniques is the difficulty in parameterizing the toolpath in terms of arc length. The discrepancy between the spline parameter and the actual arc length results in undesired feed fluctuations during real time interpolation. Feed fluctuations can bring high accelerations and jerks to the motor and lead to possibilities of drive excitations, finally deteriorating the overall curve or surface accuracy. Many researchers have developed interpolation algorithms to deal with the parametric curves. In the early years of the use of parametric curves in CNC machines, Shpitalni and Koren [2, 3] proposed Taylor's expansion to develop the first-order and the second-order interpolation algorithm while maintaining the constant feedrate. However, the method is only effective when the curve is sufficiently smooth and at least the first derivative of the curve is continuous. The curve fitting would encounter numerical issues when the curve has small radii of curvature. For mapping non-arc-length parameterized curve, Heng and Erkorkmaz [5] supposed feed correction polynomial. A single 7th order polynomial may be insufficient in some certain cases. They stated that using multiple feed correction polynomials would approximate the relationship better than increasing the order of the polynomial. In order to keep the chord error within an acceptable range, Yeh and Hsu [23] presented the adaptive feedrate interpolator in which the feed is changed adaptively according to the radius of curvature at each point on the curve

In machining processes, optimization of feed profiles also plays a major role in achieving the high precision of freeform parts. The feed modulation needs to be able to travel adaptively along the toolpath in consideration of the local curvature while preserving the physical constraints of the machine tools. Weck et al. [6] presented a worst-case optimization technique in which the maximum allowable feedrate for each segment is computed using the velocity limit, acceleration limit and jerk limit of the machine tool. The method has a straightforward formulation and requires short time of computation so it is convenient in real time CNC interpolators. Since at some sections of the curve the higher feasible

feeds are not selected as the utilized ones, the total cycle time is not totally optimized. Hence, Erkorkmaz and Altinas [8] proposed a feedrate optimization technique which uses a gradient based search to find the shortest cycle time within the kinematic and dynamic limits of the machine tools. Further, Heng and Erkorkmaz [5] developed the feed formulation with optimal cycle time by a heuristic search technique. Another feasible approach of feed profile generation was proposed by Lai et al. [12]. Except the feed, acceleration and jerk limits, the input constraints take into account also the chord error. The desired feed is selected as the minimum among of these values derived from the kinematic conditions.

This work used three interpolation techniques for capturing the relationship between the arc length and the spline parameter, i.e. Taylor expansion, adaptive feedrate and feed correction polynomial interpolation. The use of the selected interpolation depends on the requirement of the order continuity of the toolpath.

4.2 Natural interpolation

Natural interpolation is the straightforward method of interpolating along a given spline toolpath. In order to aim the excellent quality, the spline toolpath must be divided into multi linear segments. For each segment, the spline parameter is assumed to be proportional to the arc length increment:

$$u = \frac{l_k}{S_k} s \quad (4.1)$$

4.3 Taylor expansion interpolation

The Taylor's expansion method was first introduced by Shpitalni and Koren [2, 3]. The key idea for real-time interpolators is that the segmentation is based on subdivision of equal length. Accordingly, at each sampling time the method computes the successive values of u such that the length of each curve segment is constant. This leads to constant feedrate along the toolpath. The method is effective when the curve is sufficiently smooth and the first derivative of the curve is continuous.

The spline parameter is computed by using the first order Taylor's expansion at the sampling time constant $t_k = kT_s$, T_s is the control loop sampling time

$$u(k+1) = u(k) + \frac{T_s V(k)}{\|C^{(1)}(u)\|_{u=u(k)}} \quad (4.2)$$

where $\|\cdot\|$ denotes the Euclidean norm, $V(k) = V(t(k))$ denotes the desired feedrate at the time $t = kT_s$. If T_s is very small and the curve does not have small radii of curvature, even the first order approximation is adequate. However, when a segment of the curve changes roughly (curvature is relatively large), we may use two terms of Taylor's expansion.

$$u(k+1) = u(k) + \frac{T_s V(k)}{\|C^{(1)}(u(k))\|} - \frac{T_s^2 V(k)^2 C^{(1)}(u(k)) C^{(2)}(u(k))}{2 \|C^{(1)}(u(k))\|^4} \quad (4.3)$$

Once the new value of spline parameter u has been obtained, it is substituted in equation (3.1) to calculate for the next reference command point $x_{k+1}, y_{k+1}, z_{k+1}$.

Although the first and the second order Taylor's expansion are widely used in real time interpolation for CNC machines. These approximations are not reliable when the feed is varying. In addition, the existence of the derivative computation and a square root operation increases the computational load. Moreover, the method is not reliable when the feed is varying because of the accumulation of numerical error.

4.4 Feed correction polynomial

In general, NURBS toolpath parameterization does not yield accurately arc length parameterized curve. In order to avoid unwanted feed fluctuations, Erkorkmaz and Altinas [4] proposed feed correction polynomial to map non-arc-length parameterized parametric curve. The relationship between the arc length s and the spline parameter u is approximated by a 7th order polynomial.

4.5 Adaptive feedrate

The Taylor's expansion allows yielding exact results for spline parameter when the curve is smooth enough. If the radii of curvature are varying on the curve, using a constant feedrate during the machining process would lead to high chord error. In order to hold the chord error within an acceptable range, Yeh and Hsu [23] determined the relation between the feed and the chord error. Accordingly, the feed can be changed adaptively depending on the radii of curvature. The adaptive law is proposed by applying the circular approximation and using Pythagorean theorem for expressing the relation between the radius of curvature, the feed and the chord error:

$$V(u_i) = \begin{cases} F & \text{if } \frac{2}{T_s} \sqrt{\rho_i^2 - (\rho_i - ER)^2} > F \\ \frac{2}{T_s} \sqrt{\rho_i^2 - (\rho_i - ER)^2} & \text{if } \frac{2}{T_s} \sqrt{\rho_i^2 - (\rho_i - ER)^2} \leq F \end{cases} \quad (4.4)$$

NURBS interpolation and feedrate planning

where T_s is the sampling time, ER is the tolerance value of the chord error, ρ_i is the radius of curvature of the i -th interpolated point and given as the reciprocal of curvature.

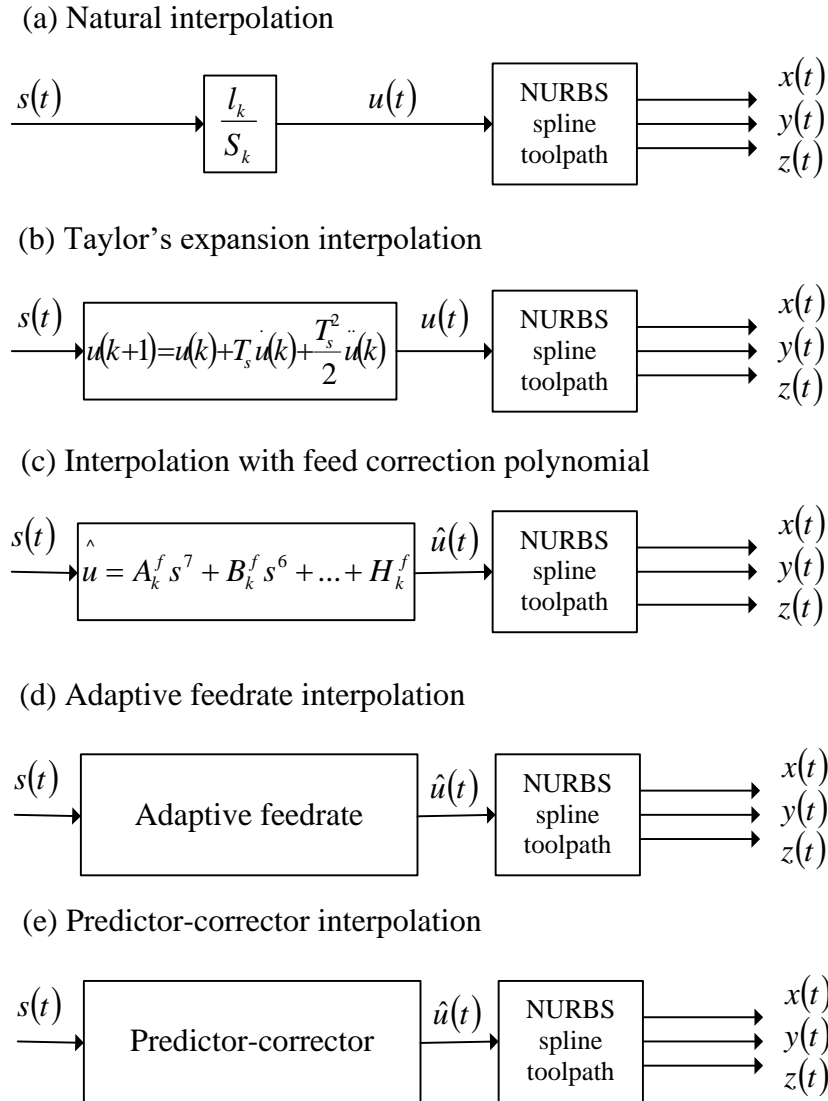


Figure 4.1: Interpolation methods used for NURBS spline toolpath

4.6 Feedrate scheduling

Improving the performance of machining process requires researchers to study the fields: geometric tools for representing parametric curve (surface), interpolation methods for reducing feedrate fluctuation and kinematic feedrate planning for preserving the physical limitations of machine tool and optimizing the machining cycle time. This subchapter will discuss about the common methods used for feed scheduling.

4.6.1 Bang-Coast-Bang acceleration profile

Bang-coast-bang acceleration profile takes into accounts the limits on velocity and acceleration. Along the segment, the feed is accelerated in the rising phase and decelerated to zero value in the falling phase. The duration of acceleration and deceleration phase must be equal in order to stop the system at the end. If the displacement is long enough, the maximum feed will be reached. After this point the system moves at a constant value. The velocity profile that corresponds to bang- coast-bang profile has a trapezoidal shape. This type of velocity profile is often used to schedule the toolpath along the straight line or smooth curve.

4.6.2 Jerk limited profile

In order to generate smoother trajectory abrupt jump of acceleration and deceleration impulse in a bang-coast-bang feed profile is replaced by ramping up and down. The velocity profile corresponds to ramping acceleration has an S-curve shape and the displacement is a cubic function of the switch times. In general, the jerk limited profile has twice of the switch times in comparison to bang-coast-bang profile. Since most real systems tend to excite vibration due to flexible components, S-curve velocity profile is often used to smoothen trajectory. Brief descriptions of the conditions for jerk, acceleration, deceleration and travel length was presented by Ekorkmaz and Altinas [7].

4.6.3 Worst case technique

The objective of feed optimization is to minimize the total time of machining process (the total cycle time) while adhering to the physical constraints of machine tool. In other words, the aim is to maximize the feedrate along the overall toolpath. Worst case technique is the feedrate optimization technique developed for spline toolpath with jerk limited profile and is commonly used in industry. The method proposed by Weck et al. [6] computes the maximum allowable feedrate for each segment based on the worst case curvature of the given toolpath. The maximum allowable feed taking the kinematic constraints of the machine tools for each toolpath segment is selected the lowest value among the feeds derived from the velocity, acceleration, jerk limits

$$f \leq \min(f_{vel}, f_{acc}, f_{jerk}) \quad (4.5)$$

Chapter 5 Identification of system parameters

5.1 Introduction

During the machining process, position tracking of the endpoint is recorded using the KGM 182 grid encoder with the accuracy of $2[\mu m]$. This work utilized the high precision of the measuring tool to identify accurately the system parameters. In addition to the grid encoder, MEMS accelerometers can be considered as the helpful measuring tool for parameter identification. They have been used for many applications in industry due to their size, cost and improved performance. Of course, for the system requires with high precision positioning, the use of the high accuracy tool is irreplaceable in terms of trajectory tracking. Nevertheless, if we only need to estimate the parameters of the specific model, MEMS accelerometers act as the suitable option. In this chapter, we will compare the usability of the mentioned tools.

5.2 Grid encoder

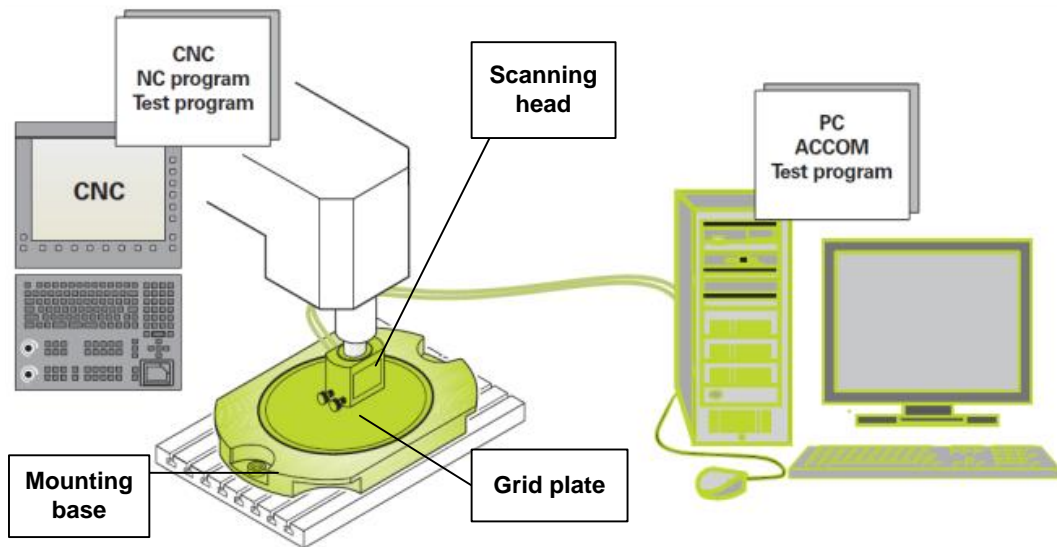


Figure 5.1: Configuration setup for inspecting a machine tool [26]

Since the KGM 182 grid encoder records the position tracking of the tool tip, we can utilize the high precision of the measuring tool to identify the parameters of the system vibration. Let Λ be the logarithmic decrement of the amplitude ratio. Equation (5.1) expresses the formula for computing the damping ratio coefficient if two successive maximums of the vibration amplitude are known.

$$\zeta = \frac{\Lambda}{\sqrt{1 + 4\pi^2 n^2}} \quad (5.1)$$

Identification of system parameters

The damped angular natural frequency ω_d is obtained by a simple formula:

$$\omega_d = \frac{2\pi}{T_d} \quad (5.2)$$

The angular natural frequency ω_n is obtained by using equation (5.3):

$$\omega_d = \omega_n \sqrt{1 - \zeta^2} \quad (5.3)$$

The data were measured at the sampling period of $0.21[ms]$. For the specified movement of $40[mm]$ along the axis in the direction x and y , the deviations of the position response are plotted out in Figure 5.2 and 5.3. The residual vibration response at the x axis expresses fairly different from the characteristics of damped vibration. This may be caused by the other structural modes of vibration. Power spectral density depicted in Figure 5.4 states that the system at the x axis has more than one mode of vibration. The system are vibrated at the frequencies $f_{nx} = 4, 30, 54[Hz]$. By applying equations (5.2), (5.3), (5.4), we see that the system oscillation is dominantly affected by the structural mode of the frequency $f_{nx} = 33[Hz]$ and damping ratio $\zeta_x = 0.75$. For the y axis drive, the system vibrates dominantly at the frequency $f_{ny} = 31[Hz]$, $\zeta_y = 0.65$.

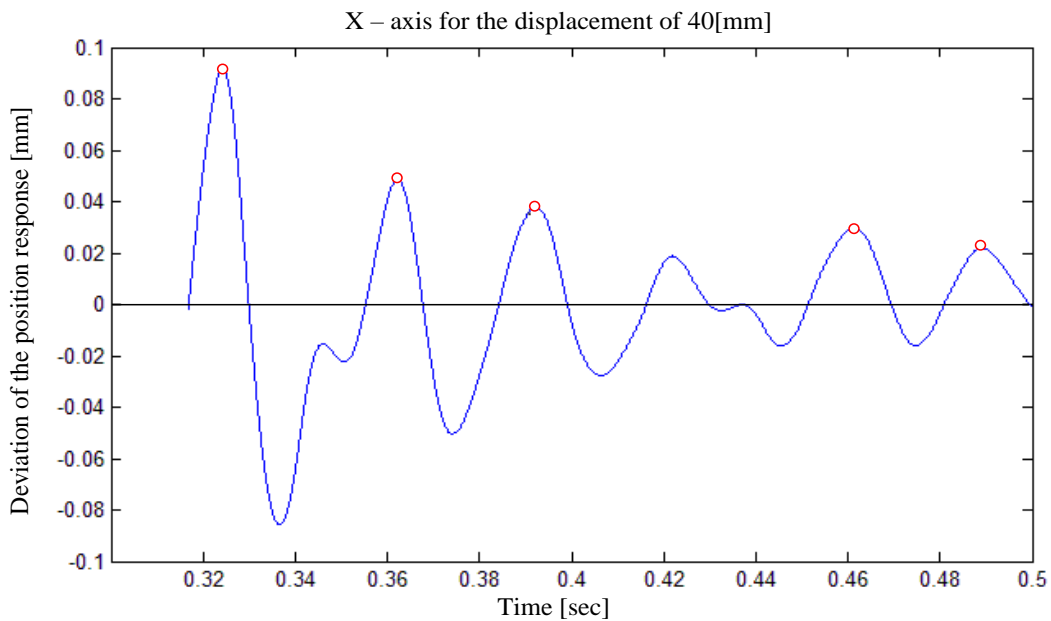


Figure 5.2: Deviation of the position response along the x axis

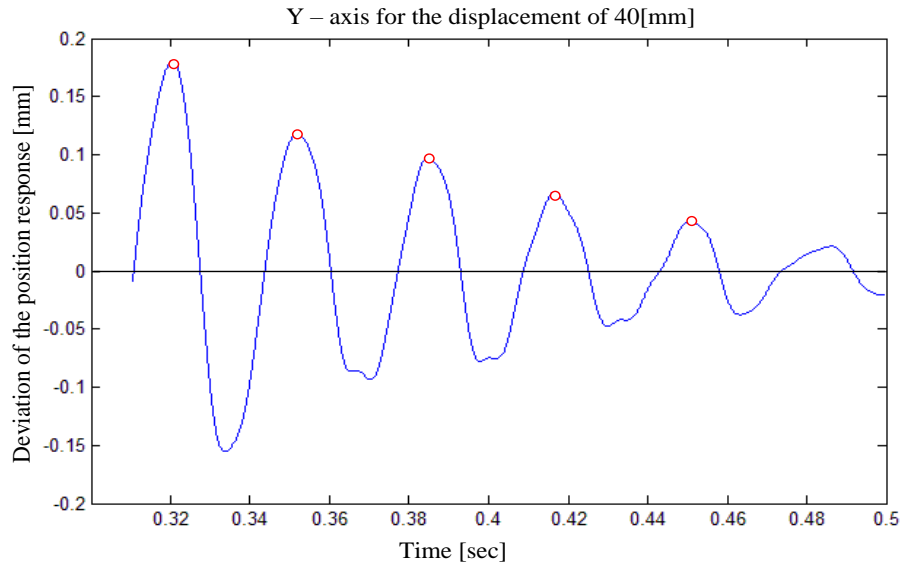


Figure 5.3: Deviation of the position response along the y axis

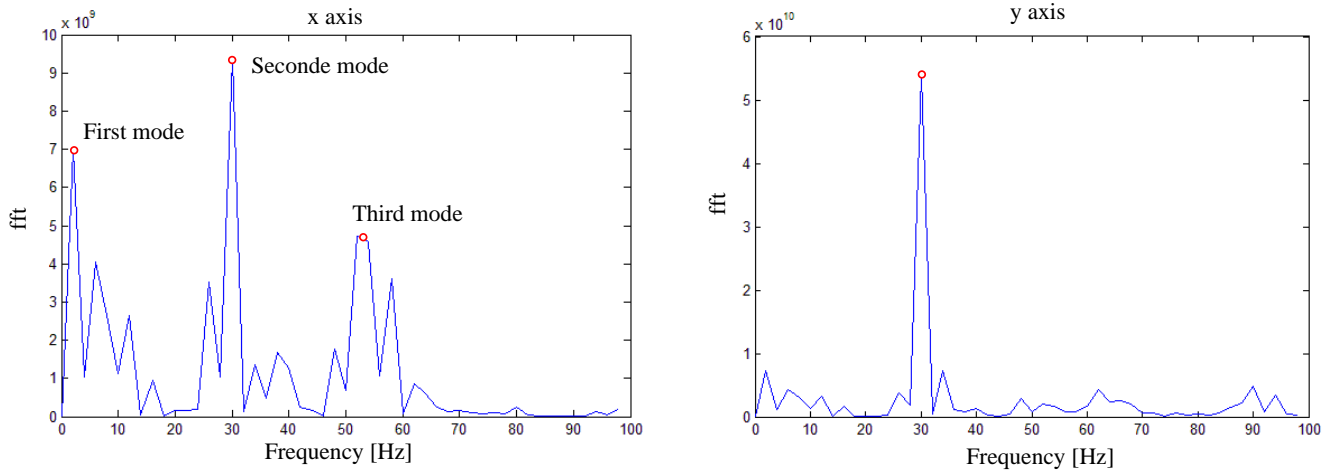


Figure 5.4: Power spectral amplitude at the x and y axes

5.3 Accelerometer

Accelerometers are sensors which are used to measure acceleration, tilt, vibration in performance driven applications. Most accelerometers are Micro-Electro-Mechanical Sensors (MEMS). Thanks to their reduced size, weight, cost and improved performance, MEMS inertial accelerometers are rapidly utilized in many applications. The basic principle of operation behind the MEMS accelerometer is that of a simple spring mass system. For sensing the displacement, a variety of transduction mechanisms have been used in accelerometers. They include capacitive, piezoresistive, electromagnetic, piezoelectric, ferroelectric, optical and tunneling. The most successful devices are based on capacitive transduction because of the simplicity, less noise, low power consumption and good stability over temperature. A typical accelerometer uses analog or digital output which is proportional to the value of acceleration.



Figure 5.5: The STM32F3DISCOVERY board mounting for acceleration measurements

The measured acceleration was obtained from the 3D digital linear acceleration sensor and 3D digital magnetic sensor LSM303DLHC. The sensor is integrated into the STM32F3DISCOVERY board that is mounted to the endpoint of the machine tool (Figure 5.5). The 32-bit ARM® Cortex™-M4 mixed-signal MCU controls the motion sensor through the I2C interface. The output data was saved by selecting the sampling rate of 400Hz and the linear acceleration full scale of $\pm 2g$. Acceleration calibration is not necessary for our applications because the LSM303DLHC has been factory-calibrated. The raw data are transferred from the device to the host through the Virtual COM port. Figure 5.6 depicts the measured accelerations when the machine tool moves along the X and Y axes, respectively. The frequency content shows the same natural frequency of vibration obtained by using the high precision of the KGM 182 grid encoder. At the last time interval, the measured acceleration expresses explicitly as the typical damped oscillation. By reading out the maximum values of acceleration and applying equations (5.1), (5.2), (5.3) the natural frequency of vibration and damping ratio are approximated to $f_{nx} = 32[Hz]$, $\zeta_x = 0.078$ for the X axis and $f_{ny} = 31[Hz]$, $\zeta_y = 0.071$

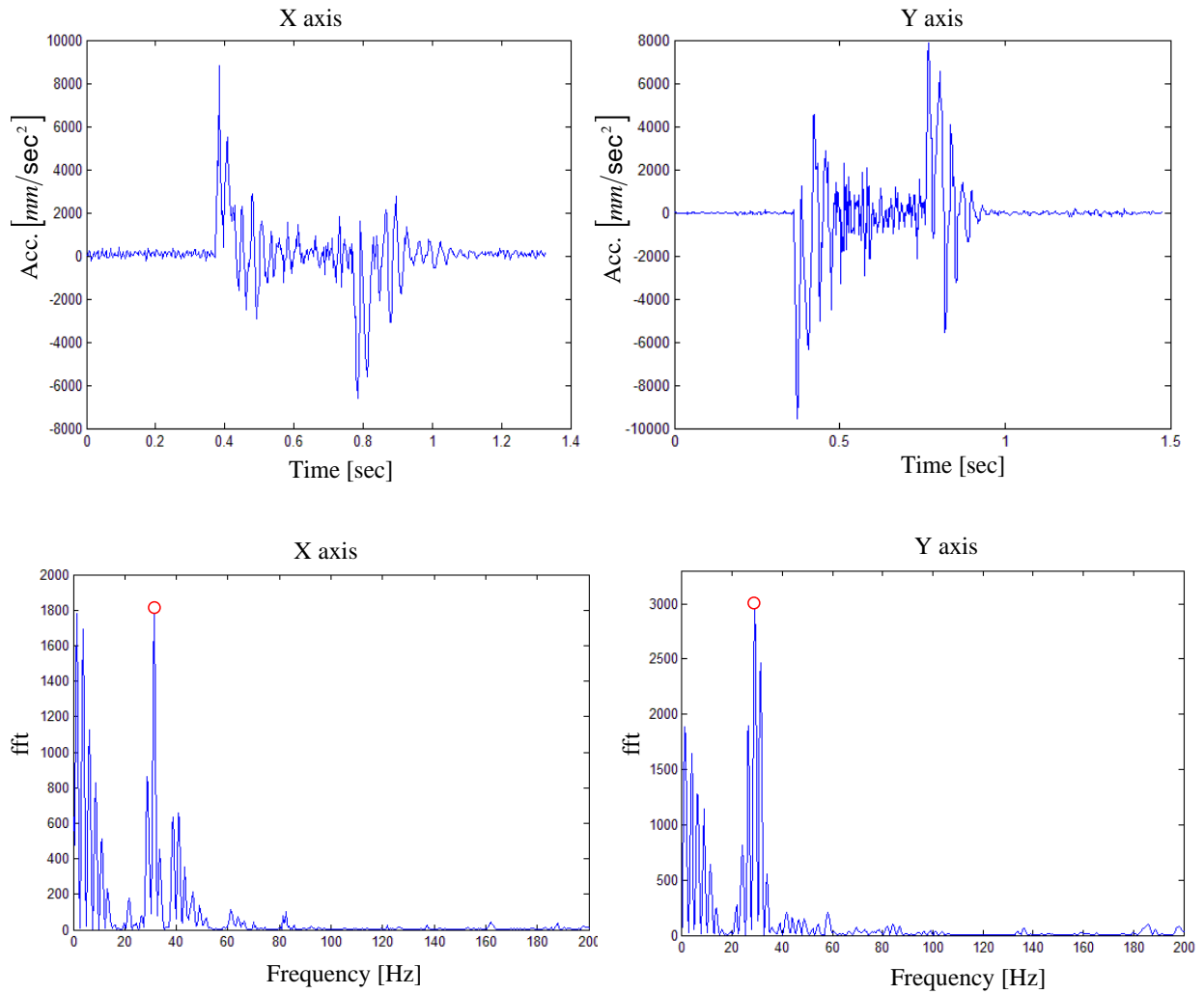


Figure 5.6: Measured accelerations and power spectral density for the X and Y axis drive

In comparison to the results obtained from the KGM 182 grid encoder, we can conclude that the low cost accelerometer allows identifying the same properties of vibration for the given system. For some specific cases, it is very helpful. For instance, when the machine is affected by an unexpected disturbance, the frequency of the structural mode can differ slightly from the original. Instead of using the high cost machining tool, the accelerometer also provides the same results.

Chapter 6 Simulations

6.1 Introduction

In this chapter, we will define tracking and contouring error that are used for evaluating the machining quality in CNC systems. Based on these types of error, objective functions of GA method are constructed for solving the shaper parameters. The dynamics of axis feed drive was included to the simulations for inspecting the excessive limits of machine tools e.g., control signal, acceleration. However, they can be figured by position derivatives. Since the controlled plant has dynamic delay in the closed loop system, zero phase error tracking control was used to improve the tracking performance [24]. The feed commands were generated by using trapezoidal or jerk limited profile considering the physical limits of machine tools. Further, the consecutive reference positions are computed at every sampling time using NURBS interpolation and sent to the position loop of CNC servo system. The effectiveness of the input shaping technique will be investigated in terms of two-dimensional trajectory following i.e. the square, the circle, the ∞ shape and arbitrary NURBS curve. Various types of input shaper were applied and compared by means of tracking and contouring error. For square toolpath the feed command profile was generated as profile to drive the system from point to point. There is no requirement of knowledge about NURBS curve representation. For circular toolpath, the radius of curvature at every point on the circle is identical. Thus, Taylor's expansion is a good fitting for NURBS circular toolpath. The following section tested adaptive feedrate interpolator for the ∞ shaped toolpath. In the final simulation, arbitrary NURBS toolpath uses feed correction polynomial interpolation to produce feedrate with no fluctuation.

6.2 Tracking and contouring error

In machining processes, tracking and contouring errors are given as the two performance indices for evaluating the precision of machine tool. Tracking error is the deviation between the reference point and the actual point. Tracking error can be improved by applying the feedback and feedforward controller to each axis individually, such as a large P position controller or ZPETC (zero phase error tracking controller). Contouring error is defined as the error component orthogonal to the desired trajectory (the shortest distance from the desired trajectory to the actual position).

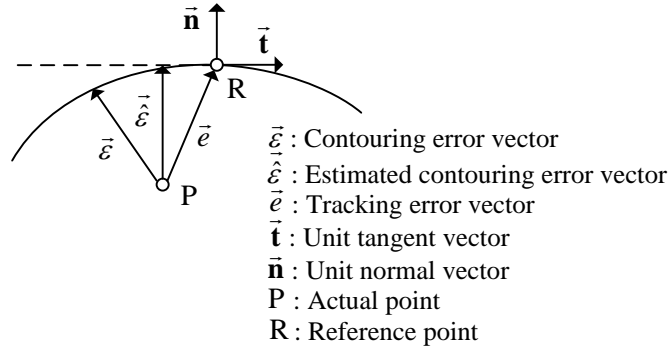


Figure 6.1: Geometrical representation of tracking and contouring error

The expression for estimated contouring error vector is derived as:

$$\vec{\hat{\epsilon}} = \langle \vec{e}, \vec{n} \rangle \vec{n} \quad (6.1)$$

where $\langle \cdot \rangle$ is the inner product. For general multi-axis machining system, contour error vector can be estimated using the task coordinate frame (shifted Frenet frame) which is attached to the desired contour and change its orientation at every point on the curve. The task coordinate frame is comprised of the mutually orthogonal unit tangent \vec{t} , normal \vec{n} and bi-normal $\vec{b} = \vec{t} \times \vec{n}$. A good approximation of contour error vector can be given as:

$$\vec{\epsilon} \cong \vec{e}_n + \vec{e}_b \quad (6.2)$$

where \vec{e}_n , \vec{e}_b are two components of the tracking error \vec{e} corresponding to \vec{t} and \vec{b} axis, mapped from the physical coordinate frame composed of $\{\vec{e}_1, \vec{e}_2, \vec{e}_3\}$ to the task coordinate frame constructed of $\{\vec{t}, \vec{n}, \vec{b}\}$.

The objective function can be formed as the sum of estimated contouring errors or velocity errors along the overall toolpath.

$$OF1 = \sum_{i=1}^n \hat{\epsilon}_i \quad (6.3)$$

$$OF2 = \sum_{i=1}^n |f_{di} - f_{ai}| \quad (6.4)$$

where $\hat{\epsilon}_i$ is the estimated contour error at the i -th point

f_{di} , f_{ai} is the desired and actual feedrate at the i -th point

6.3 Drive controller

In conventional multi-axial system, each axis is controlled by a separate closed loop control. In the simulations, each axis drive was implemented by the proportional (P) position controller cascaded with proportional-integral (PI) velocity controller. For improving the tracking accuracy, the feed-forward controller (ZPETC) was also added to cancel the phase shift for all frequencies.

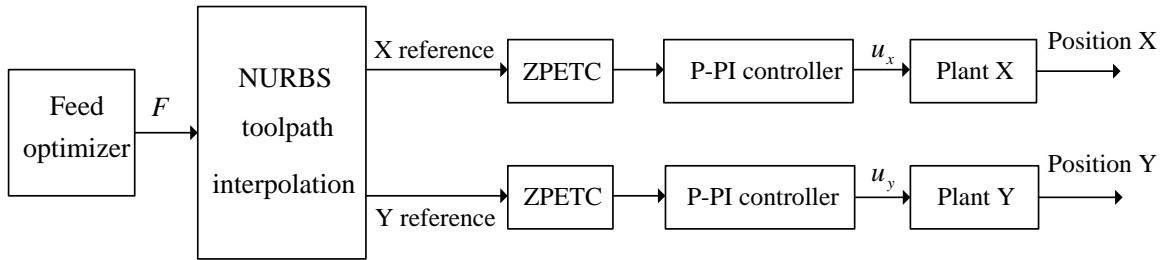


Figure 6.2: P-Pi + ZPETC controller for axis feed drives

Although the designed toolpath for the CAD/CAM system is fairly smooth, short transient phase of acceleration or the presence of flexible components can still lead the system to structural excitation mode. The machine tool was modeled at the structural mode of vibration with natural frequencies $f_{nx} = 33Hz$, $f_{ny} = 31Hz$ and damping ratios $\zeta_x = 0.075$, $\zeta_y = 0.065$.

6.4 Square

Machining tool travelling along the square with the dimension of $50 \times 50 [mm \times mm]$ was simulated. The maximum values of jerk were set within the limits $J_x = J_y = 80000 [mm/sec^3]$, the tangential jerk limit was $J = 50000 [mm/sec^3]$. The axis velocity limits were set equal to $f_{xmax} = f_{ymax} = 250 [mm/sec]$. The axis velocity maximum was set to $f_{xmax} = f_{ymax} = 141.67 [mm/s]$ and acceleration maximum was set to $a_{xmax} = a_{ymax} = 3000 [mm/sec^2]$ in both x and y directions. The control signal was set within the limit $\pm 8[V]$. The sampling time used for the machining tool controlling was set to $T_s = 0.5 [msec]$. The machining process was supposed to be started from the origin $(0, 0)$ with a departure angle 0^0 in direction +X and then in direction +Y.

In order to obtain the desired point, Singhose [25] proposed a simple improvement by adding a delay time equal to the shaper length in the process when the system moves from one corner to the next one. By doing that the tool tip reaches to zero value at the corners. Nevertheless, zero valued feed at the corners may be unacceptable for high speed machining with a laser beam. This work proposes another solution by employing genetic algorithms based shaper. This type of input shaper helps to reduce system vibration amplitudes and minimize the contouring error within the allowable tolerance. The

solution does not require any improvement at the corner so the total time of machining process is reduced in three times of the shaper length. On the second hand, the corners are punished qualitatively in terms of the rounding issue and insensitivity. As the typical problem of input shaping, a delay time must be added at the end to complete the machining process. As seen in Figure 6.3, the maximum peak of the feed amplitude was reduced in percentage from 12.4 down to 0.7 and the maximum contouring error was remarked from 0.1191 [mm] to 0.023 [mm].

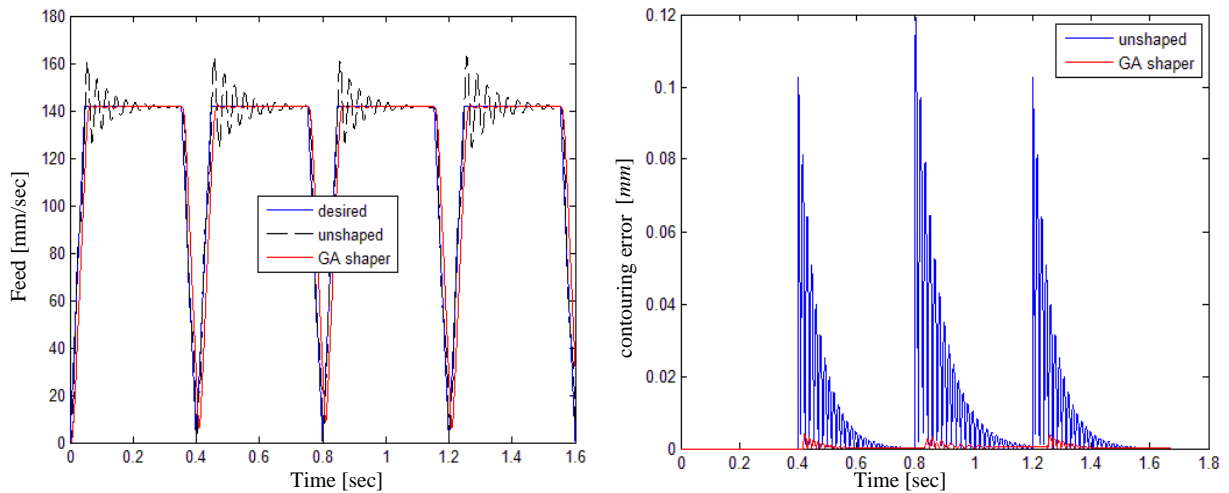


Figure 6.3: Square response to unshaped, GA shaped position commands

6.5 Circle

A full circle with the center at $(0, R)$ and radius $R = 25[mm]$ was generated by using NURBS technique. The full circle is constructed based on the nine-point square:

$$\{\mathbf{P}_i\} = \left\{ \begin{bmatrix} 0 \\ 0 \end{bmatrix}, \begin{bmatrix} 25 \\ 0 \end{bmatrix}, \begin{bmatrix} 25 \\ 25 \end{bmatrix}, \begin{bmatrix} 25 \\ 50 \end{bmatrix}, \begin{bmatrix} 0 \\ 50 \end{bmatrix}, \begin{bmatrix} -25 \\ 50 \end{bmatrix}, \begin{bmatrix} -25 \\ 25 \end{bmatrix}, \begin{bmatrix} -25 \\ 0 \end{bmatrix}, \begin{bmatrix} 0 \\ 0 \end{bmatrix} \right\} \begin{matrix} [mm] \\ [mm] \end{matrix}$$

weight coefficients:

$$\{w_i\} = \left\{ 1, \frac{\sqrt{2}}{2}, 1, \frac{\sqrt{2}}{2}, 1, \frac{\sqrt{2}}{2}, 1, \frac{\sqrt{2}}{2}, 1 \right\}$$

and knots:

$$U = \left\{ 0, 0, 0, \frac{1}{4}, \frac{1}{4}, \frac{1}{2}, \frac{1}{2}, \frac{3}{4}, \frac{3}{4}, 1, 1, 1 \right\}$$

The circle is $\mathbf{C}^0, \mathbf{C}^1$ continuous and was initiated from point $\mathbf{P}_0(0,0)$ in the $+x$ direction with resultant constant feedrate $f = 141.67[mm/s]$. The total travelling length of the toolpath is simply computed for circular case, that is $L = 2\pi R = 157.0796[mm]$. Since the radius of curvature at every point on the circle is identical, the feed can track at a fixed value. Taylor's expansion interpolation is a good fitting for circular shape. The feed command profile was scheduled such that the tool tip starts

Simulations

using an energy beam after acceleration phase and ends prior to deceleration phase during the machining process.

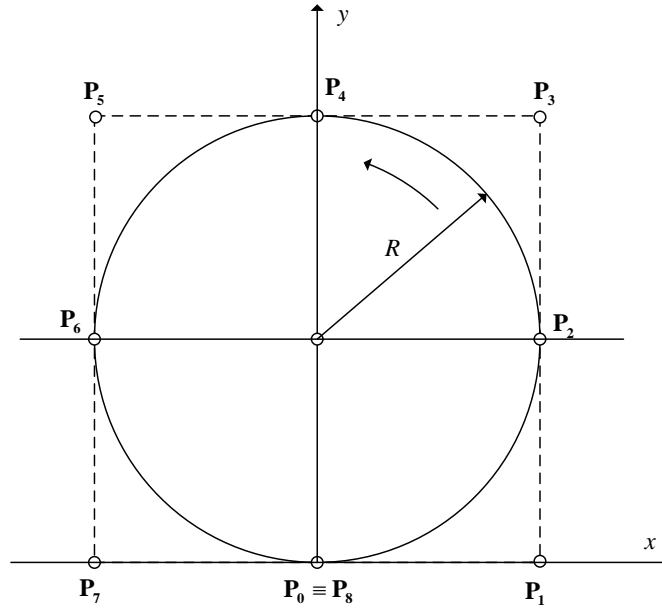


Figure 6.4: A full NURBS circle using nine control polygons

Two S-functions were created in Simulink to compute the basis functions and derivatives of the NURBS toolpath. The source code was written in C language based on the C MEX file template [sfuntmpl_basic.c](#). Consecutive reference points sent to CNC machines are evaluated based on first order Taylor's expansion interpolation.

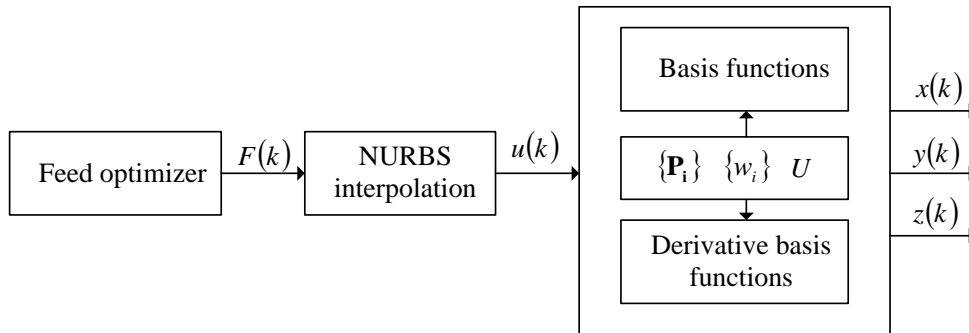


Figure 6.5: Schematic diagram of NURBS toolpath position

In simulations, ZVD, ZP and GA shaped feed commands were tested to compare the effectiveness of input shaping to that without input shaping. Objective functions were computed based on position following (6.3) and feed following (6.4). Although the shaper parameters designed for x and y axes are nearly the same, the convolution of two shapers ensures both axes are shaped with the same xy shaper. The resultant shaper consists of nine impulses contributed within the total shaper length $(T_x + T_y)$.

$$\begin{bmatrix} A_{xy} \\ T_{xy} \end{bmatrix} = \text{conv} \left(\begin{bmatrix} A_x \\ T_x \end{bmatrix}, \begin{bmatrix} A_y \\ T_y \end{bmatrix} \right) \quad (6.5)$$

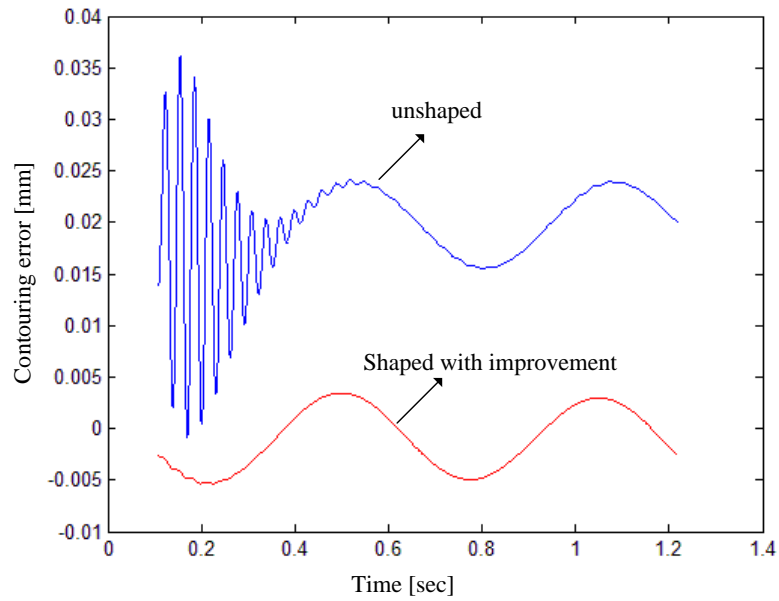


Figure 6.6: Comparison of contouring error for unshaped and ZVD shaped circular trajectory

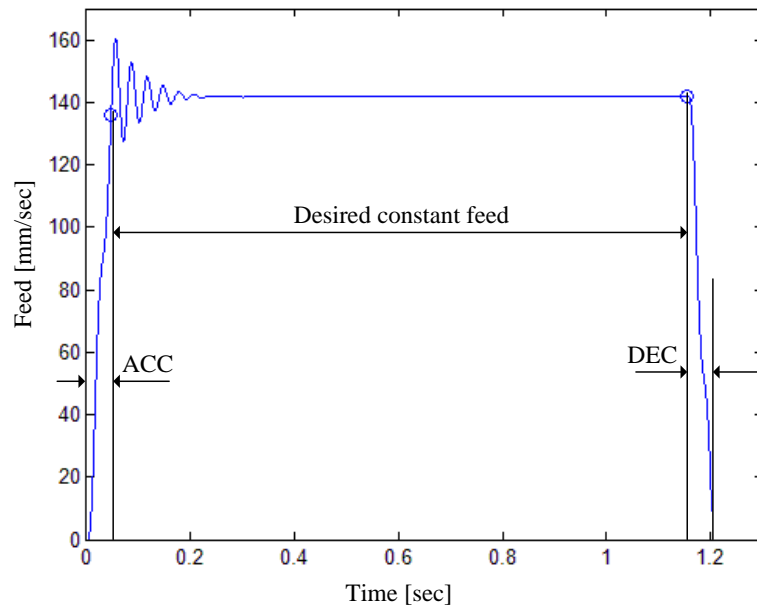


Figure 6.7: Feed response of biaxial vibration system to unshaped feed command

6.6 The ∞ shape toolpath

In this subsection, the toolpath was generated by using the ordinal control points

$$\{\mathbf{P}_i\} = \left\{ \begin{bmatrix} 0 \\ 0 \end{bmatrix}, \begin{bmatrix} -60 \\ -60 \end{bmatrix}, \begin{bmatrix} -60 \\ 60 \end{bmatrix}, \begin{bmatrix} 0 \\ 0 \end{bmatrix}, \begin{bmatrix} 60 \\ -60 \end{bmatrix}, \begin{bmatrix} 60 \\ 60 \end{bmatrix}, \begin{bmatrix} 0 \\ 0 \end{bmatrix} \right\} \begin{bmatrix} mm \\ mm \end{bmatrix}$$

weight vector

$$\{w_i\} = \{1, 25, 25, 1, 25, 25, 1\}$$

Simulations

and knot vector

$$U = \left\{ 0, 0, 0, \frac{1}{4}, \frac{1}{2}, \frac{1}{2}, \frac{3}{4}, 1, 1, 1 \right\}$$

The total length of ∞ shape curve using adaptive quadrature method was approximated to $L = 505.673[\text{mm}]$ within the specified tolerance of $\varepsilon = 1e-8$. The curve is $\mathbf{C}^0, \mathbf{C}^1$ continuous and was initiated from point $\mathbf{P}_0(0,0)$ in the $-x$ direction with the same maximum feedrate as for square and circular trajectory $f = 141.67[\text{mm/s}]$ (see Figure 6.8)

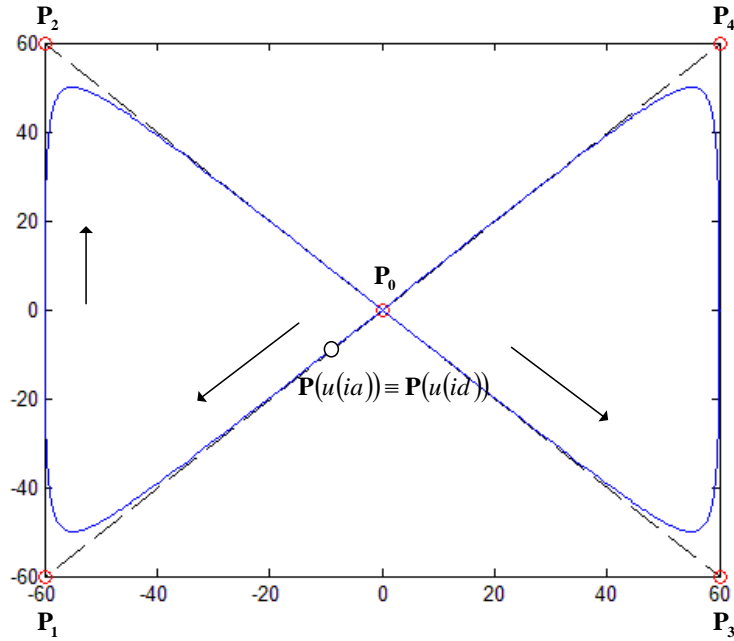


Figure 6.8: The ∞ shape curve and control points

Three various types of feed profile were simulated to investigate the important role of feed planning:

- a) the ACC/DEC stage included feed profile,
- b) constant feed profile,
- c) curvature dependent feed profile.

The curvature dependent feed profile uses the ACC/DEC realization outside the machining process with the aim of achieving the maximum desired feedrate. This work employed the idea of [23] to generate the adaptive feed profile with consideration of the curvature. ia , id are the number of sampling time steps which correspond to initial time and end time of machining process respectively. The first order Taylor's interpolation was used to evaluate the spline parameter for the next sampling step.

Figure 6.9 indicated that feed scheduling plays also an important role as other aspects for precise machining such as interpolation methods, control technique of feed drives. ZVD, GA based shapers

Simulations

were applied and compared to the unshaped input commands. GA based shapers allow minimizing contouring errors based on their objective functions. Although GA based shapers do not eliminate the vibration drastically, their performance of vibration reduction is still remarkable compared to that without shaping.

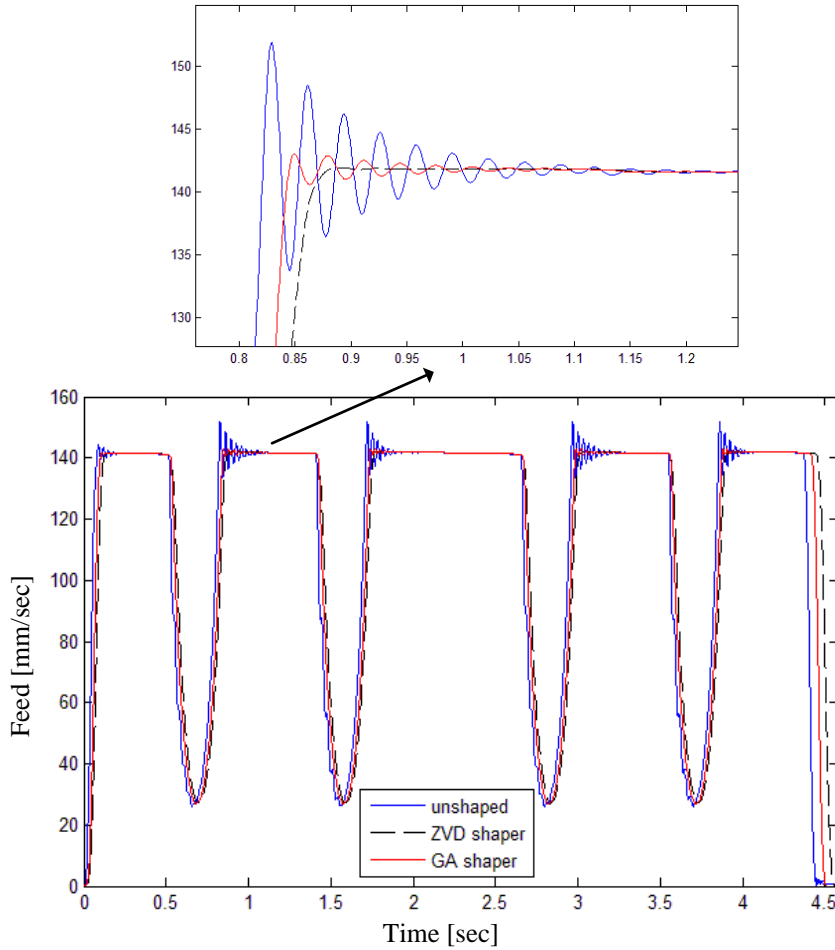


Figure 6.9: Feed response of adaptive feed profile to ZVD and GA shaped position commands

6.7 Arbitrary shape toolpath

Figure 6.11 shows a cubic ($p = 3$) NURBS curve generated by nine control points:

$$\{P_i\} = \left\{ \begin{bmatrix} 0 \\ 0 \end{bmatrix}, \begin{bmatrix} 10 \\ 40 \end{bmatrix}, \begin{bmatrix} 50 \\ 70 \end{bmatrix}, \begin{bmatrix} 60 \\ 40 \end{bmatrix}, \begin{bmatrix} 65 \\ 0 \end{bmatrix}, \begin{bmatrix} 90 \\ 0 \end{bmatrix}, \begin{bmatrix} 110 \\ 0 \end{bmatrix}, \begin{bmatrix} 120 \\ 30 \end{bmatrix}, \begin{bmatrix} 100 \\ 50 \end{bmatrix} \right\} \begin{matrix} mm \\ mm \end{matrix}$$

weight coefficient vector:

$$W = [1, 1, 1, 1, 1, 1, 1, 1, 1]$$

and knot vector:

$$U = [0, 0, 0, 0, 0.2, 0.4, 0.6, 0.8, 0.9, 1, 1, 1, 1]$$

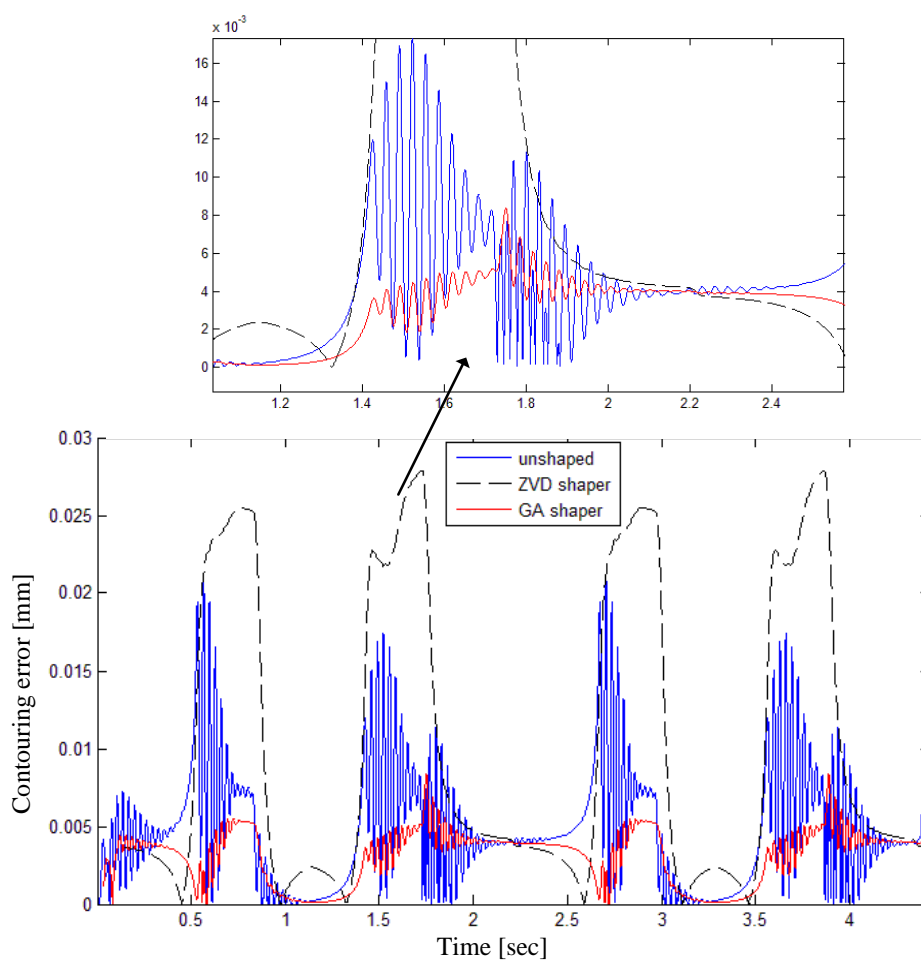


Figure 6.10: Contouring error response of adaptive feed profile to ZVD and GA shaped position command

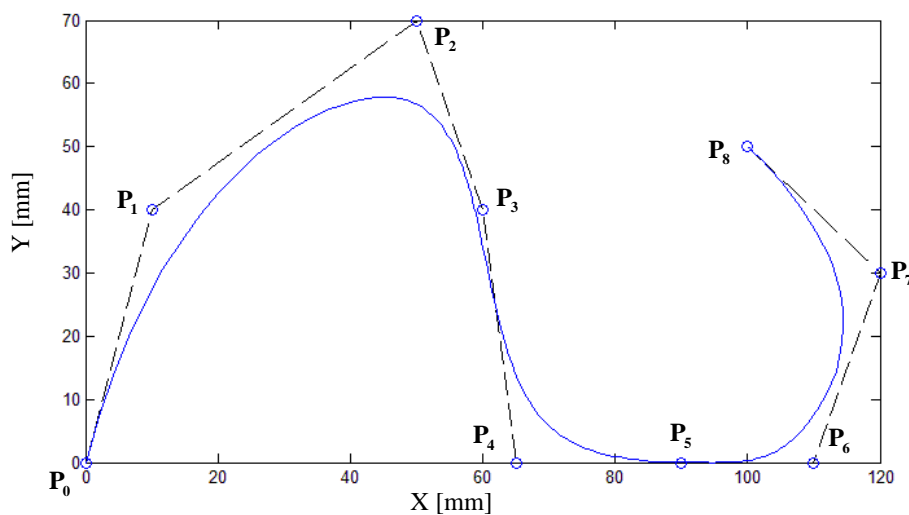


Figure 6.11: An arbitrary NURBS curve constructed by nine control points

The curve is C^0, C^1, C^2 continuous over the knot interval. Using adaptive quadrature method the total length of the curve was approximated to $L = 230.442[mm]$ within the specified tolerance of $\varepsilon = 1e-8$. The machine tool was considered as to travel along the given NURBS toolpath with the feed

profile generated by the worst-case method. For each segment the feed was modulated using piecewise constant jerk values which results in S-curve type transitions (jerk limited profile).

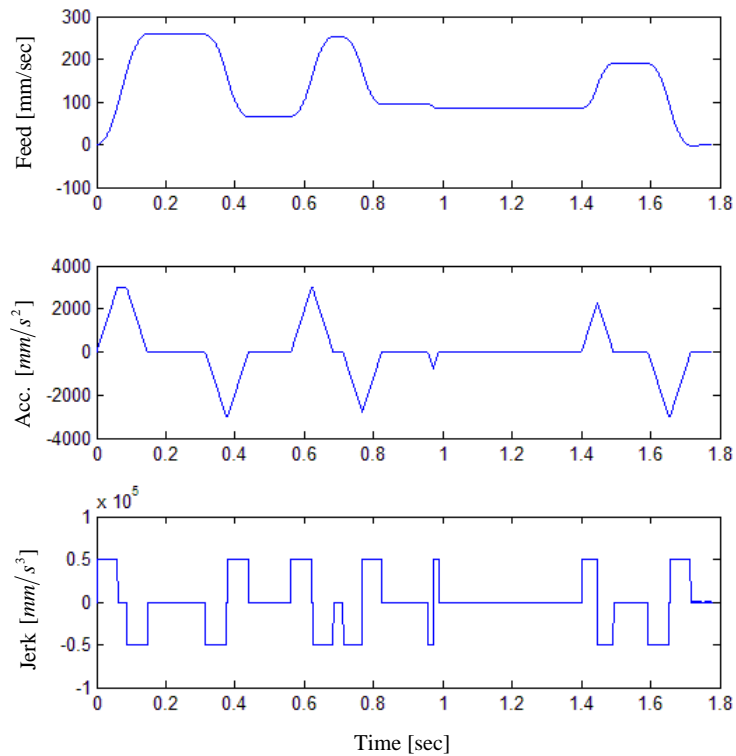


Figure 6.12: Feed profile generation of the worst-case method

The feed response showed that ZVD shaper is effectively suppressed the residual vibration. However, the obtained results of contouring errors are unexpectedly higher at high curvature points on the toolpath. This is caused by the basic problem of input shaping. As the result of using input shaping, the total feed generation is delayed by a shaper length. At high curvature points, the feed is required to decrease as planned. Actually, it changes a short time later. Delay time response to the feed profile causes the increase in contouring errors. If the total sum of contouring errors along the given toolpath is a matter of interest, the GA based shaper can be applied to investigate as for the ∞ toolpath case. Input shaper containing three impulses was added to pre-shape the position commands. For increasing robustness to the modeling error a number of impulses in the impulse sequence can be increased.

Figure 6.13 and 6.14 depicted that GA based input shaping performs remarkable decrease in contouring errors and vibration. However, input shaper causes a delay in the overall system. To complete the machining process, the shaper length must be added to machining cycle time.

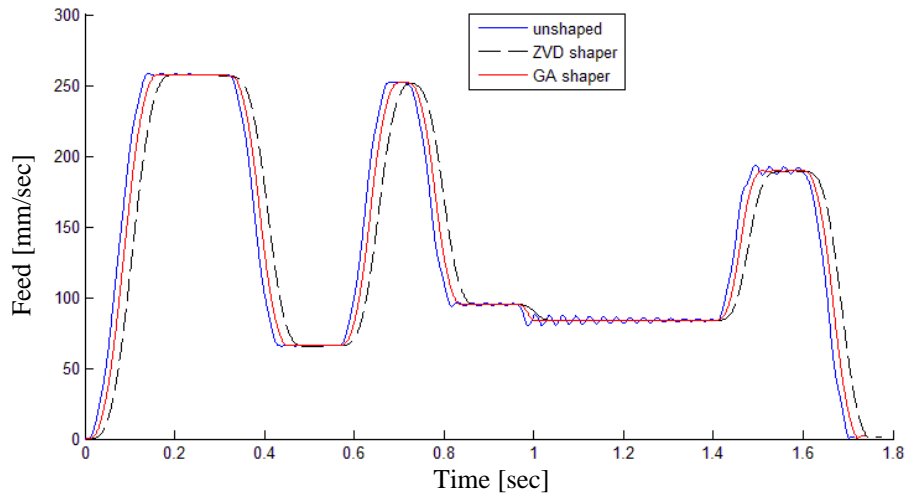


Figure 6.13: Feed response to unshaped, ZVD and GA shaped position commands

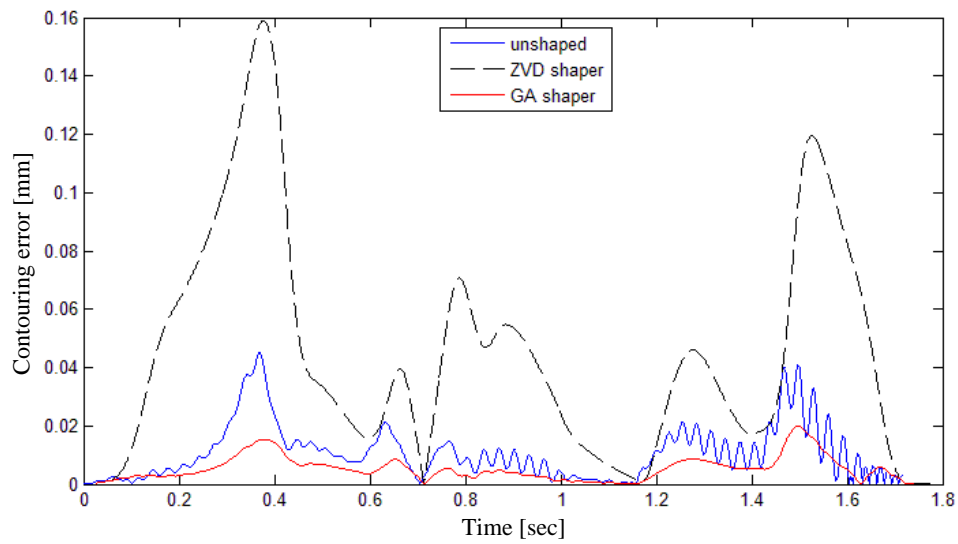


Figure 6.14: Contouring error response to unshaped, ZVD and GA shaped position commands

Chapter 7 Experimental results

7.1 Hardware

The real time implementation of the simulated toolpaths was conducted on a high speed biaxial CNC machine using laser MSF1863 as shown in Figure 7.1. The axial position feedbacks are sampled through two encoders with a resolution of 32500[imp/rev] and used for servo position control. Measured positions used for machining evaluation are obtained by the KGM 182 grid encoder with a resolution of 2[μm]. The scanning head is vertically mounted at the tool tip and the mounting base is fixed on the X-Y table.

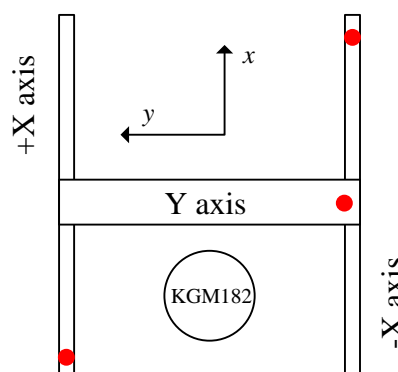


Figure 7.1: Implementation of biaxial CNC machine

For achieving high accuracy the motion in x axis is driven by two motors while y axis is driven by one motor. The maximum speed of servos in the x, y axis is 4500 [rev/min] and 5000 [rev/min] respectively. The shaped positions generated by Matlab/Simulink were used to send as input position

commands for the CNC feed drives. Because the actuators drive the system in each axis with an accuracy of $1[\mu m]$, so the generated positions are necessary to be rounded up to $1[\mu m]$.

7.2 Square

Figure 7.2 and 7.3 showed that input shaping performs as well as the results obtained by simulations. Position commands were altered to eliminate the possibility of the structural mode. The reduction of the frequency content prevents the system to excite during the machining process along the square toolpath. The maximum contouring errors were reduced from $0.1442[mm]$ of unshaped to $0.0554[mm]$ of shaped positions. It is noticed that contouring errors oscillates around the average value of $0.04[mm]$ when travelling from the second corner to the next one. This may come from the numerical rounding errors. As stated previously, the position commands sent to the feed drives are rounded off to $1[\mu m]$. Numerical rounding causes slightly residual vibration of position response. To improve the accuracy, the desired position commands for y axis can be reduced by around $0.04[mm]$, that is $49.96[mm]$.

Different type of input shapers were compared to investigate the efficiency of input shaping on vibration reduction. In addition, the S-curve velocity generation was also used for the purpose of transient phase smoothing. The experimental results indicated the similar response of the square to ZVD, EI and ZP shaped positions. Figure 7.4 shows the spectral amplitude at the structural mode of excitation has been reduced completely for both x and y axis. The system has high power spectral density to vibrate at $f_{nx} = 4[Hz]$ for the x direction. The results can even be improved if we take into consideration the first low mode of vibration. The resultant shaper is obtained by the convolution of individual shapers for each mode. Of course, the shaper length is increased and equal to the sum of individual shaper lengths.

7.3 Circle

The effectiveness of input shaping on circular trajectory following was discussed by previously published papers. The experiments were implemented only with the aim of verifying. Figure 7.6 showed the oscillated feedrate was reduced significantly during the machining process when applying input shaper. The spectral amplitudes for both x and y axis in Figure 7.7 have also verified this statement. Due to vibration, the unshaped velocity response is slightly smaller compared to the desired command. In terms of contouring errors, circular trajectory tracking with the radius of $R = 25[mm]$ was not improved clearly. The unexpected contouring error response may come from the mutual dynamic effects among two axes or inappropriate selection of multiplication gain.

Experimental results

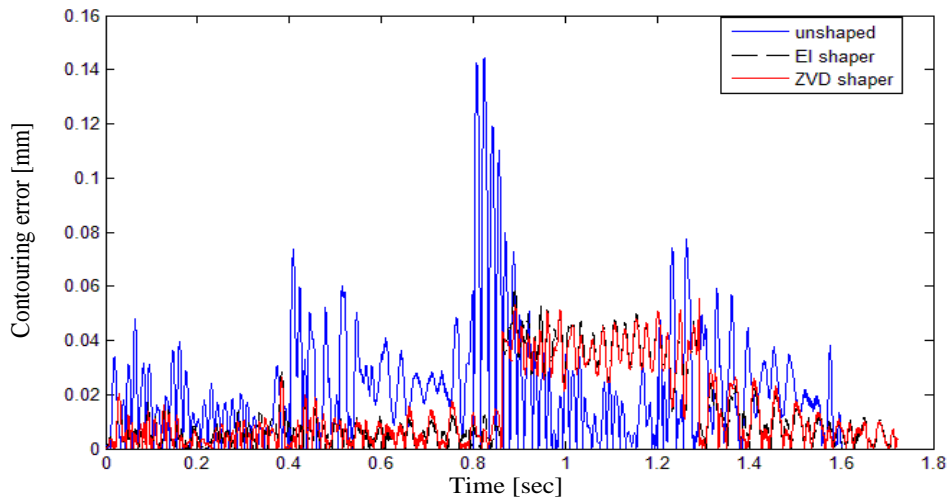


Figure 7.2: Contouring error response of the square to unshaped, EI and ZVD shaped positions

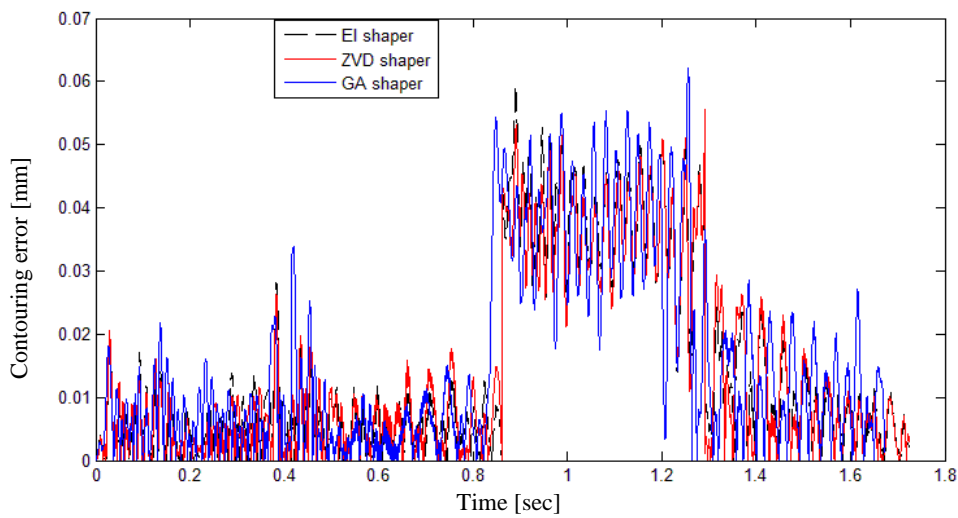


Figure 7.3: Contouring error response of the square to EI, ZVD and GA shaped position

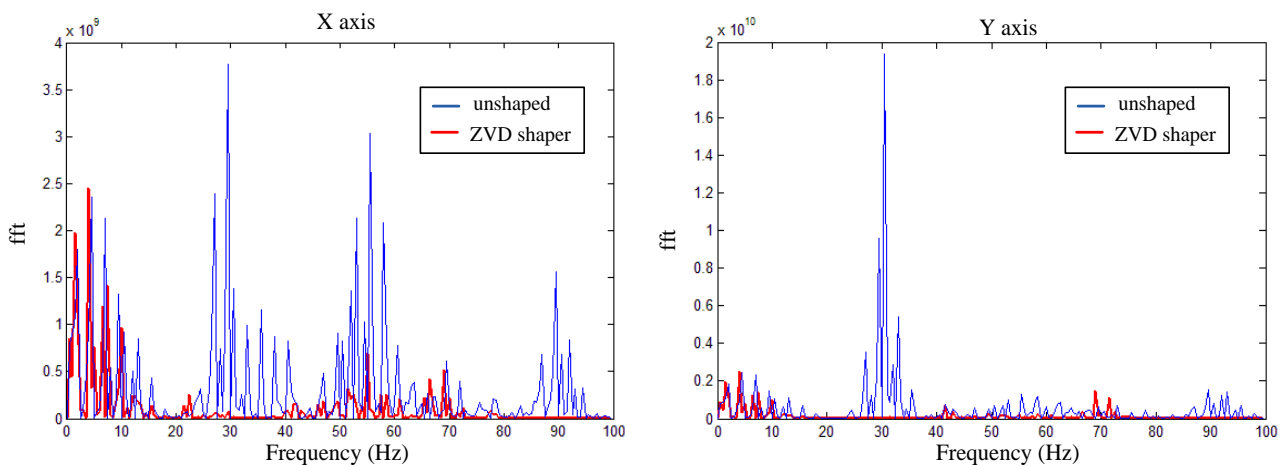


Figure 7.4: Power spectral density of unshaped and ZVD shaped square

Experimental results

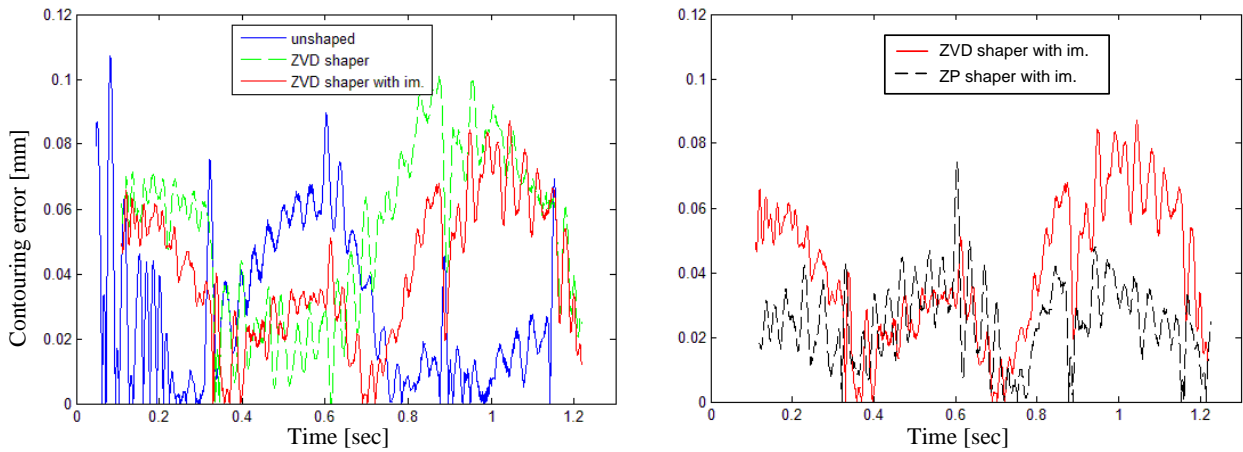


Figure 7.5: Contouring error response of the circle to unshaped; ZVD, ZP shaped positions

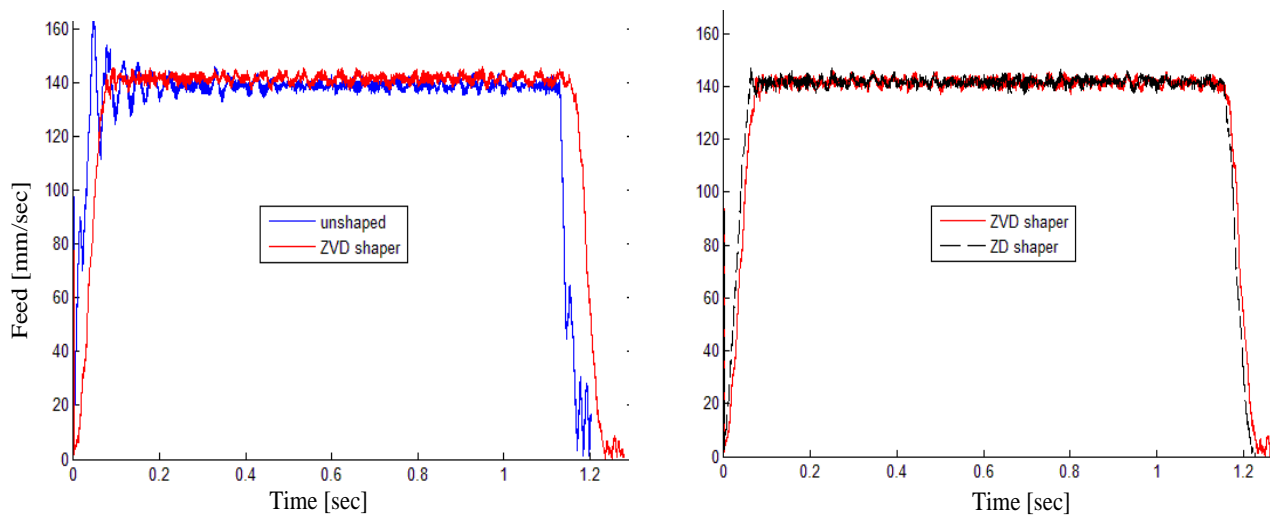


Figure 7.6: Feed response of the circle to unshaped, ZVD, ZP shaped position commands

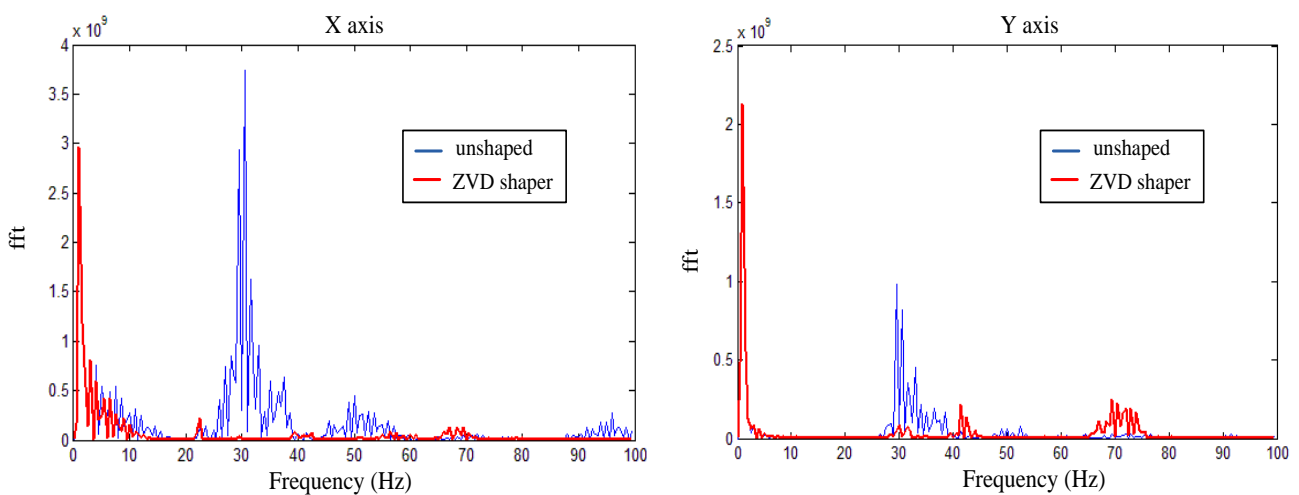


Figure 7.7: Power spectral amplitude of unshaped and ZVD shaped circle

7.4 The ∞ shape toolpath

The feed profiling plays the important role of the curvature varying toolpath in the accuracy. Fixed feedrate tracking along the ∞ shape toolpath causes high contouring errors and high residual vibration, especially at high curvature points as depicted in Figure 7.8 and 7.9. Using input shaping technique, the vibrated speed is suppressed significantly. However, the reduction in maximum contouring error is not remarked. Shaper delay leads to higher tracking errors. Therefore, at some short segments with high curvature this disadvantage of input shaping results in higher chord errors. Contouring errors were obtained extremely small even for unshaped position commands when employing adaptive method. Position command using a zero displacement technique showed as the most effective shaper in terms of contouring error (Figure 7.10 and 7.11). The experimental results have performed as well as the results obtained from simulations. Hence, better results can be expected when using genetic algorithm based shaper as discussed in simulation part. Since the machine tools are owned by the private company, until the time of dissertation finalizing the author did not have enough time to verify all the measurement as planned. Nevertheless, the effectiveness of GA based shaper on trajectory following was proven to the arbitrary toolpath.

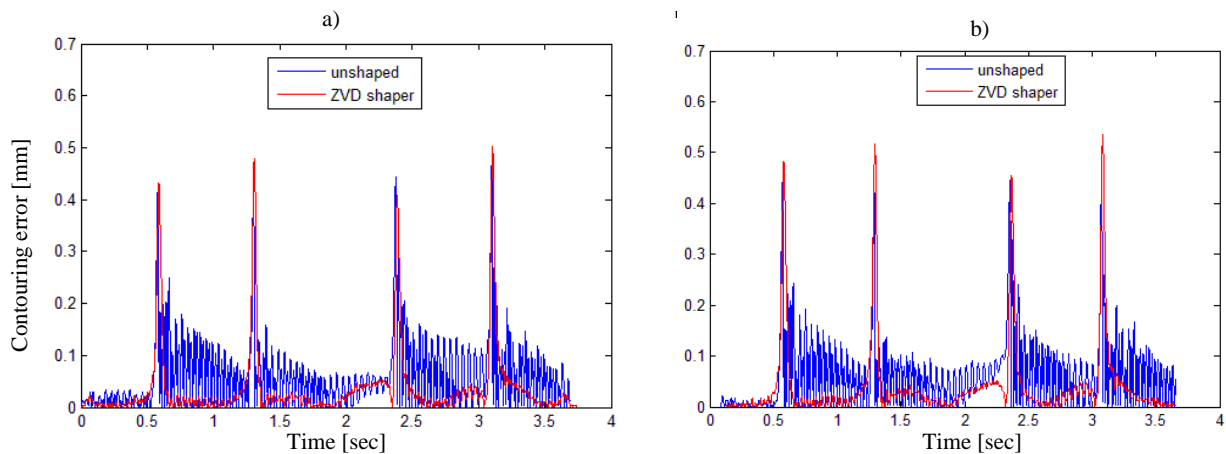


Figure 7.8: Contouring error response of the ∞ shape toolpath to unshaped and ZVD shaped position commands: a) ACC/DEC realization including feed profile, b) Constant feed profile

Experimental results

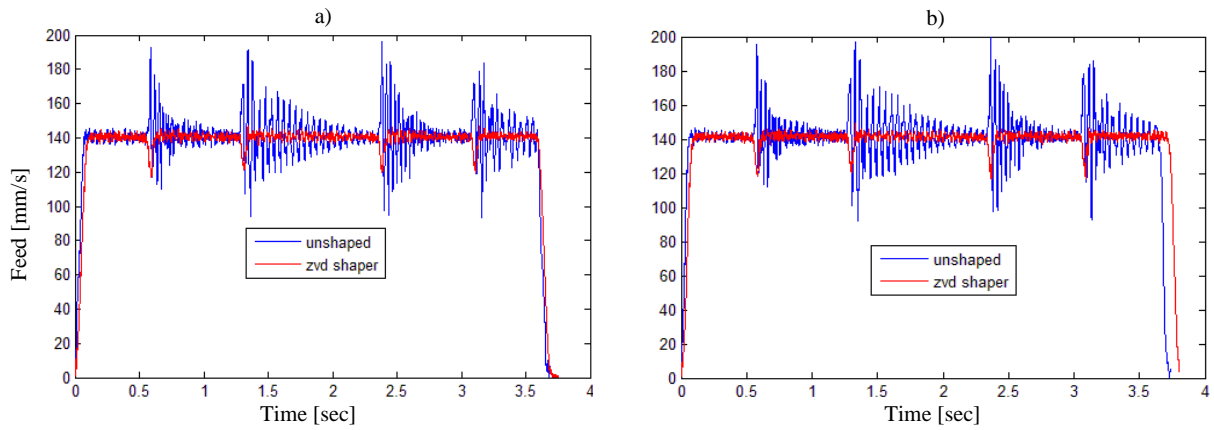


Figure 7.9: Feed response of the ∞ shape toolpath to ZVD shaped position commands: a) ACC/DEC realization including feed profile, b) Constant feed profile

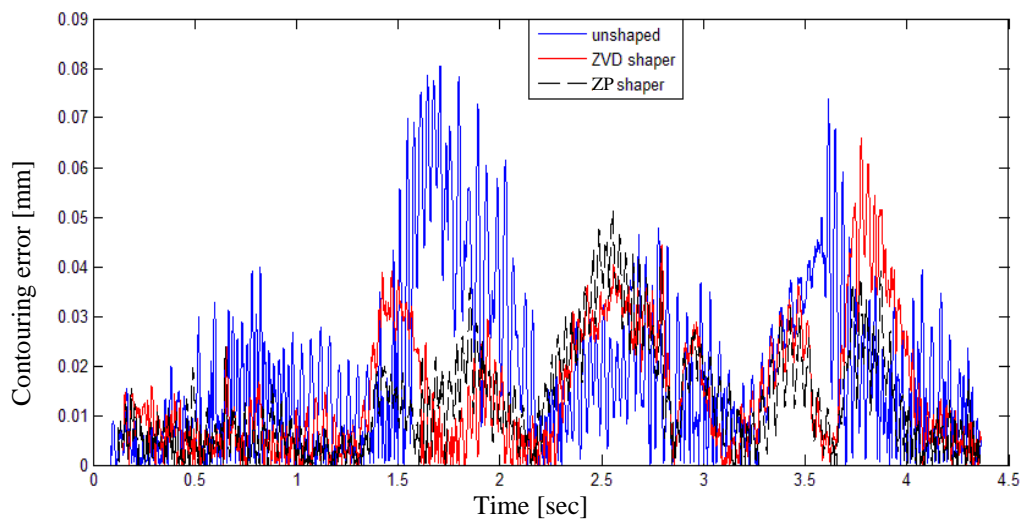


Figure 7.10: Contouring error response of adaptive feed profile to unshaped, ZVD and ZP shaped position commands

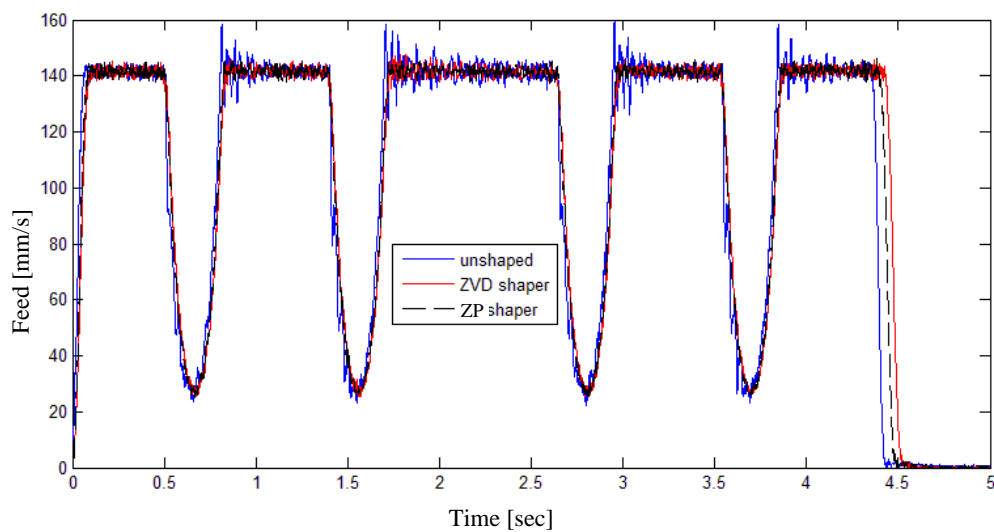


Figure 7.11: Feed response of adaptive feed profile to unshaped, ZVD and ZP shaped position commands

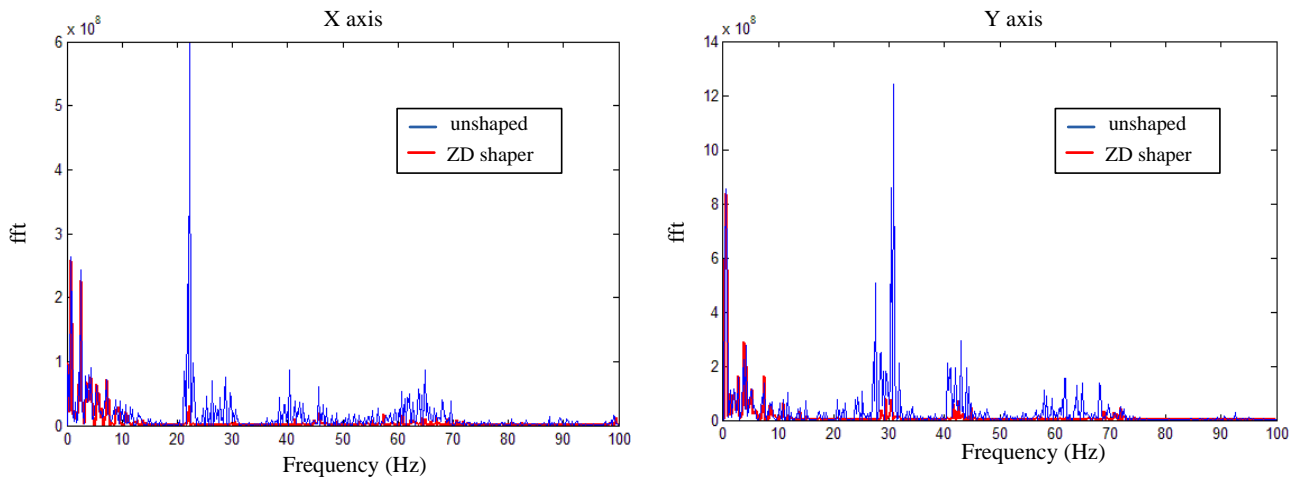


Figure 7.12: Power spectral density of unshaped and ZD shaped positions using adaptive feed profile

7.5 Arbitrary toolpath

The practicality of GA based input shaper was proven to the arbitrary toolpath compared to traditional shapers in terms of contouring error following. The experimentally verified method can be applied to any multi-axis machine tools. In Figure 7.14, the maximum contouring error was reduced from the unshaped peak of $0.116 [mm]$ to the GA shaped peak of $0.07 [mm]$. Figure 7.15 plotted the power spectral amplitude. Again, it is stated that relevant feed scheduling helps to avoid the machine tool's structural mode. In comparison to the square toolpath, the spectral amplitude density of the arbitrary toolpath is suppressed and has lower power to vibrate. At the points with high curvature corresponding to the times at around $t = 0.35 [s]$ and $t = 1.48 [s]$, the interpolated toolpath tracking has the maximum in contouring errors. It is caused by a slow transition for the feed among the segments. As the proposed shaper attempts to minimize the sum of contouring errors, the GA shaped feed was not suppressed as well as ZVD or ZP shaped profile. On the second hand, the length of the GA based shaper is shorter, so the feed responds to the GA shaped command faster.

Experimental results

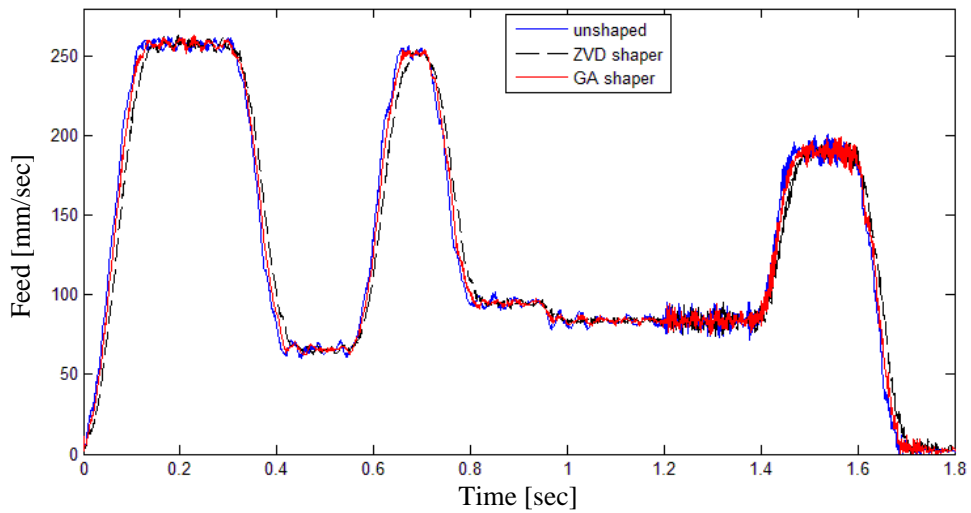


Figure 7.13: Feed response of worst-case generation profile to unshaped, ZVD and GA shaped positions

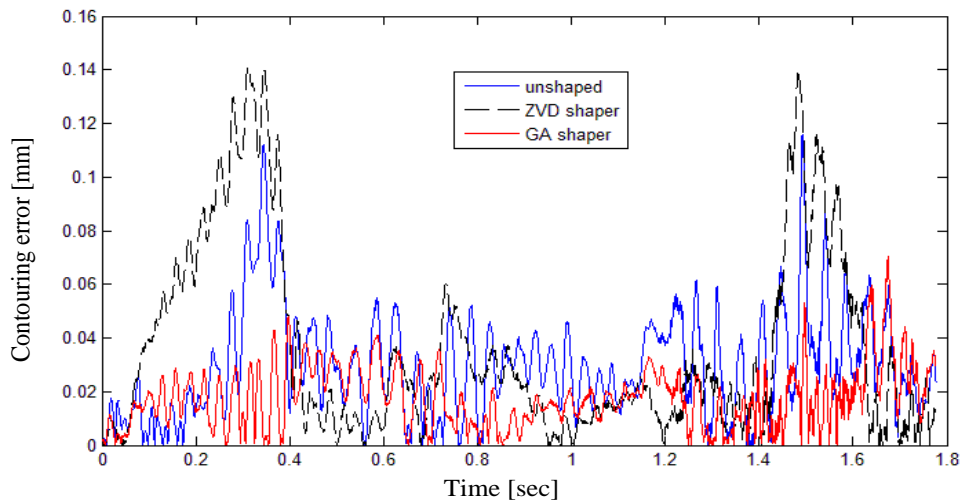


Figure 7.14: Contouring error response of worst-case generation profile to unshaped, ZVD and GA shaped positions

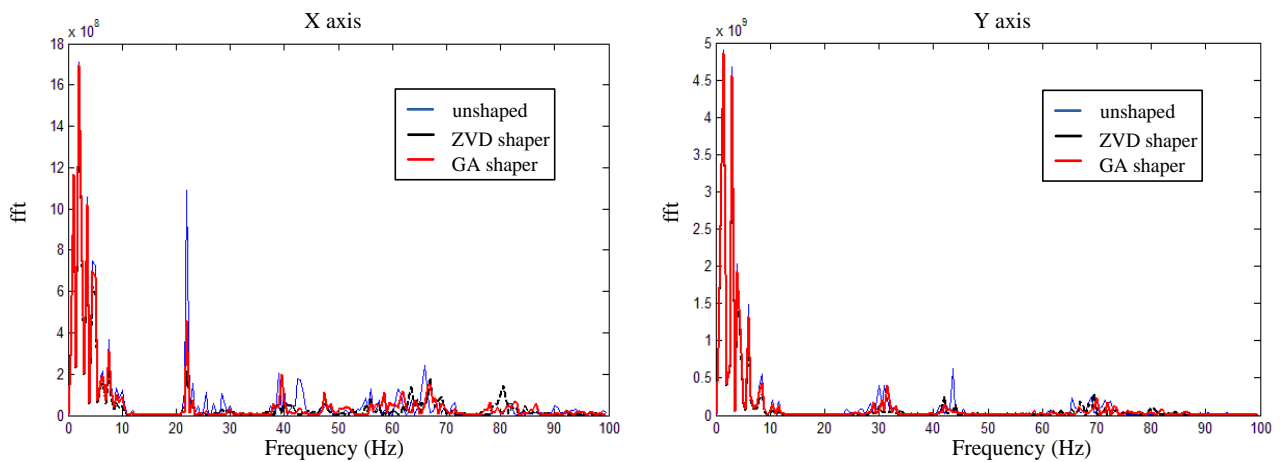


Figure 7.15: Power spectral density of unshaped, ZVD and GA shaped arbitrary toolpath

CONCLUSIONS

High speed multi-axis machining requires interpolated position commands with high frequency content in acceleration and jerk. Due to the structural mode of the drives, the endpoint of machine tools exhibits the problem of vibration. Vibration elimination aims at better quality in curve (surface) finish. In this work, NURBS curve representation was adopted to generate smooth trajectories. Unlike conventional interpolation such as linear and circular interpolation, NURBS interpolation offers higher geometric continuity which prevents abrupt jumps in the axis velocity profile. In addition, the feed profiles were generated using S-curve transition which allows reducing high frequency content in jerk. The adaptive feed and the worst-case method considering the kinematic limits of machine tools were chosen to change the velocity adaptively depending on the curvatures at every interpolated point. Because of the existence of flexible components, the overall mechatronic systems still have the tendency to oscillate. Input shaping was used to investigate the effectiveness of vibration reduction on two dimensional following. The experiments were conducted on high speed bi-axial CNC system with a laser which belongs to the company Microstep s.r.o. The system parameters of vibration for the given mechatronic system were identified using both the KGM 182 grid encoder and the linear MEMS acceleration sensor. For the square and circular toolpath, contouring error response to shaped position has been decreased when using conventional shapers with simple improvements. The basic problem of input shaper is to add a delay to the overall cycle time. Based on the knowledge of input shaping technique, genetic algorithm based shapers were designed and compared to analytical shapers. For arbitrary trajectory, using shapers based on analytical method lead to worse quality in tracking errors and contouring errors. On the contrary, genetic algorithm based shapers demonstrated the advantage in terms of contouring errors. Both simulation and experimental results have proved the practicability of the proposed method. The disadvantage of using genetic algorithms is the requirements of high computation time. The experimental results were tested on the bi-axial system, but can be applied to any multi-axis configuration system.

In continuation of this work, one of the future research directions is to verify the feasibility of GA based shaper on 3D trajectory following. For multi-axial high speed machine tools, contouring errors are computed more complex using the shifted Fernet frame. The second research direction is to apply input shaping based on the analytical approach for vibration reduction. Since analytical input shapers lead to the increase in contouring errors, an additional controller is required to compensate contouring errors between axes before commanding positions to the axis drives.

REFERENCE

- [1]. Piegl, L., W. Tiller (1997), *The NURBS Book*, second ed., Springer, Berlin.
- [2]. Shpitalni, M., Y. Koren, C.C. Lo (1994), "Realtime Curve Interpolators," *Computer Aided Design*, **26**(11), pp. 832–838.
- [3]. Koren, Y. and C.C. Lo, M. Shpitalni (1993), "CNC Interpolator: Algorithm and Analysis," *ASME J. Manuf. Sci. Eng.*, **64**, pp. 83-92.
- [4]. Erkorkmaz, K., Y. Altinas (2005), "Quintic Spline Interpolation with Minimal Feed Fluctuation," *ASME J. Manuf. Sci. Eng.*, **127**(2), pp. 339-349.
- [5]. Heng, M., K. Erkorkmaz (2010), "Design of a NURBS interpolator with minimal feed fluctuation and continuous feed modulation capability," *Int. J. Mach. Tools. Manuf.*, **50**(3), pp. 281-293.
- [6]. Weck M, Meylahn A, Hardebusch C (1999), "Innovative Algorithms for Spline-Based CNC Controller," *Annals of the German Academic Society for Production Engineering*, **6**(1), pp. 83–86.
- [7]. Erkorkmaz, K., Y. Altintas (2001), "High Speed CNC System Design: Part I-Jerk Limited Trajectory Generation and Quintic Spline Interpolation," *Int. J. Mach. Tools & Manuf.*, **41**(9), pp. 1323–1345.
- [8]. Altinas, Y., K. Erkorkmaz (2003), "Feedrate Optimization for Spline Interpolation in High Speed Machine," *Annals of CIRP-Manufacturing Technology*, **52**(1), pp.297-302
- [9]. Erkorkmaz, K., M. Heng (2008), "A heuristic feedrate optimization strategy for NURBS toolpaths," *Annals of CIRP-Manufacturing Technology*, **57**(1), pp.407–410.
- [10]. Cheng, C.W, M.C. Tsai (2004), "Real-time variable feedrate NURBS curve interpolator for CNC machining," *Int. J. Adv. Manuf. Technol.*, **23**(11-12), pp.865-873.
- [11]. Lei, W.T, M.P. Sung, L.Y. Lin, J.J. Huang (2007), "Fast real-time NURBS path interpolation for CNC machine tools," *Int. Journal of Machine Tools & Manufacture*, **47**, pp. 1530-1541.
- [12]. Lai, Y.J., K. Y. Lin, S. J Tseng, W. D, Ueng (2008), "On the development of a parametric interpolator with confined chord error, federate, acceleration and jerk", *Int. J. Adv. Manuf. Technol* **37** (1-2), pp. 104-121

REFERENCE

- [13]. Zhang, Q.G, R.B. Greenway (1998), "Development and implementation of a NURBS curve motion interpolator," *Robotics and Comp.-Integrated. Manuf.*, **14**, pp. 27-36.
- [14]. Singer, N.C, W.P. Seering (1990), "Preshaping Command Inputs to Reduce SystemVibration," *ASME Journal of Dynamic System, Measurement and Control*, **112**(1), pp.76-82.
- [15]. Singhose, W.C, W.P. Seering, N.C. Singer (1990), "Shaping Inputs to Reduce Vibration: A Vector Diagram Approach," in Proc. *IEEE Int. Conference on Robotics and Automation*, pp.922-927.
- [16]. Hubinsky, P. (2000), "Control of mechatronic systems with slightly low oscillation", Slovak University of Technology, Slovakia.
- [17]. Hubinsky, P., L. Jurisica, B. Vranka (2005), "Genetic algorithm based method of elimination of residual oscillation in mechatronic systems," *Kybernetika*, **41**, pp.623-636.
- [18]. Duong, Q.K, P. Hubinsky, P. Paszto, M. Florek, J. Sovcik, M. Kajan (2014), "Effectiveness of input shaping and realtime NURBS interpolation for reducing feedrate fluctuation," *Procedia Engineering* 96, pp.81-90.
- [19]. Rattan, K.S., V. Feliu (1992), "Feedforward Control of Flexibile Manipulators," In. *Proc. the 12th IEEE International Conference on Robotics and Automation*, pp.788-793.
- [20]. Murphy, B.R., I. Watanabe (1992), "Digital Shaping Filers for Reducing Machine Vibration," *IEEE Transactions on Robotics and Automation*, **8**(2), pp.285-289.
- [21]. Tuttle, T.D., W.P. Seering (1994), "A Zero-placement Technique for Designing Shaped Inputs to Suppress Multiple-mode Vibration," In *Proc. American Control Conference*, **3**, pp.2533-2537.
- [22]. Haupt, R.L. and S.E. Haupt (2004), "Practical Genetic Algorithms," John Wiley and Sons Publication.
- [23]. Yeh S.S, P.L. Hsu (2002), "Adaptive-feedrate interpolation for parametric curves with a confined chord error," *Computer Aided Design*, **34**(3), pp.229-237.
- [24]. Tomizuka, M. (1987), "Zero phase error tracking algorithm for digital control," *ASME Journal of Dynamic Systems, Measurement and Control*, **109**, pp.65-68.
- [25]. Singhose W.E, N. C. Singer (1996) "Effectiveness of Input Shaping On Two-Dimensional Trajectory Following", *IEEE Trans. on Robotics and Automation*, **12**(6), pp.881-887.

REFERENCE

- [26]. <http://www.heidenhain.com/fileadmin/pdb/media/img/208871-28 Measuring Devices For Machine Tool Inspection and Acceptance Testing.pdf>
- [27]. <http://www.st.com/web/en/resource/technical/document/datasheet/DM00027543.pdf>
- [28]. <http://www.sensorwiki.org/doku.php/sensors/accelerometer>
- [29]. http://www.st.com/web/en/resource/technical/document/application_note/CD00268887.pdf

Publications by author

International Journals

- [1]. Sovcik, J., M. Kajan, F. Duchon, M. Florek, P. Hubinsky, K. Duong Quang (2014), “Coordinated Movement of Multiple Robots in Outdoor Environment with Obstacles,” *International Journal of Robotics and Automation Technology*, **1**(2), pp. 57-62. ISSN 2409-9694.
- [2]. Paszto, P., M. Klucik, L. Chovanec, M. Tolgyessy, J. Hanzel, K. Duong Quang, P. Hubinsky (2014), “Object Relative Position Estimation Based on Hough Transform Using One Camera,” *International Journal of Imaging and Robotics*. **13**(2), pp.1-11. ISSN 2231-525X. In database of:SCOPUS.

Conferences

- [3]. Duong Quang, K., P. Hubinsky (2013), “Genetic Algorithm Based Input Shaping on Two - Dimensional Trajectory Following,” In *ELITECH'13: 15th Conference of Doctoral Students; Bratislava, Slovakia*. ISBN 978-80-227-3947-4.
- [4]. Duong Quang, K., P. Hubinsky, P. Paszto, M. Florek, J. Sovcik, M. Kajan (2014), “Effectiveness of input shaping and real-time NURBS interpolation for reducing feedrate fluctuation,” In *Procedia Engineering: The 6th International Conference on Modelling of Mechanical and Mechatronic Systems MMaMS, Vysoke Tatry, Slovakia*, **96**, p. 81-90. ISSN 1877-7058, In database of SCOPUS.